Geochemistry Geophysics Geosystems G3

Article
Volume 13, Number 3
31 March 2012
Q03025, doi:10.1029/2011GC003887
ISSN: 1525-2027

Published by AGU and the Geochemical Society

Global variations in H_2O/Ce: 2. Relationships to arc magma geochemistry and volatile fluxes

Daniel M. Ruscitto
Department of Earth and Environmental Sciences, Rensselaer Polytechnic Institute, Troy, New York 12180, USA (ruscid2@rpi.edu)

Department of Geological Sciences, University of Oregon, Eugene, Oregon 97403, USA

Paul J. Wallace
Department of Geological Sciences, University of Oregon, Eugene, Oregon 97403, USA

Lauren B. Cooper
Department of Mineralogy, University of Geneva, CH-1205 Geneva, Switzerland

Institute for Geochemistry and Petrology, ETH-Zürich, CH-8029 Zurich, Switzerland

Terry Plank
Lamont-Doherty Earth Observatory, Columbia University, Palisades, New York 10964, USA

[1] We compiled a data set of 100 primitive arc magma compositions from melt inclusion and whole rock analyses to compare volatile contents, slab tracers, and calculated subduction component compositions between 18 subduction zone segments spanning the global range in slab thermal structure. The average primitive magma H_2O content in our data set is 3.3 ± 1.2 wt.% (1 s.d.) for melts erupted within 50 km of the volcanic front. While there is a wide range of volatile contents in magmas within individual arcs, the highest values occur in magmas erupted from vents along the volcanic front, where the subducting slab is located 104 ± 29 km (avg ± 1 s.d.) beneath the surface. This observation, coupled with positive correlations between H_2O, Cl, S, and B contents and predictions from geodynamic models, provides strong evidence for the active supply of volatile-rich slab-derived components from the subducting oceanic plate beneath volcanic arcs. We also show that temperature-sensitive ratios (e.g., H_2O/Ce) for both primitive arc magmas and calculated subduction components are similar and display monotonic behavior with slab thermal parameter. Furthermore, calculated subduction component compositions have higher trace element to H_2O ratios in arcs with hotter slabs (lower thermal parameter), suggesting that hydrous melts of differing compositions are added beneath different arcs. Finally, we present new volatile outflux estimates for Central Cascades magmatism and then compare these to estimates for the Central American and Kamchatka-Kurile arcs to create a combined data set spanning a large range in slab thermal parameter.

Components: 21,800 words, 14 figures, 3 tables.

Keywords: arc magmas; slab temperature; subduction fluids; subduction zones; volatile flux; volatiles.

Index Terms: 1030 Geochemistry: Geochemical cycles (0330); 1031 Geochemistry: Subduction zone processes (3060, 3613, 8170, 8413); 1043 Geochemistry: Fluid and melt inclusion geochemistry.

Received 23 September 2011; **Revised** 10 February 2012; **Accepted** 12 February 2012; **Published** 31 March 2012.

Ruscitto, D. M., P. J. Wallace, L. B. Cooper, and T. Plank (2012), Global variations in H_2O/Ce: 2. Relationships to arc magma geochemistry and volatile fluxes, *Geochem. Geophys. Geosyst.*, *13*, Q03025, doi:10.1029/2011GC003887.

1. Introduction

[2] Arc volcanism occurs along destructive plate margins because hydrous fluids or melts derived from the dehydrating subducting slab lower the solidus of the overlying mantle wedge and induce melting. As a result, primitive arc magmas reflect contributions from both the downgoing plate (subducted sediment, oceanic crust, and possibly serpentinized mantle) and the overlying mantle wedge [e.g., *Gill*, 1981; *Plank and Langmuir*, 1993, 1988; *Elliott*, 2003]. No single reaction is responsible for slab dehydration, rather a complex series of continuous reactions occur in response to increasing pressure and temperature conditions within the subducting plate [*Schmidt and Poli*, 1998; *Hacker*, 2008]. Previous studies have related global variations in arc volcanics to the compositions of incoming sediments and observed that arc outputs generally reflect subduction inputs [e.g., *Plank and Langmuir*, 1993]. Arc outputs should reflect other input parameters as well (e.g., age of incoming plate, dip angle). One such important subduction parameter (Φ) corresponds to the expected thermal state of the slab:

$$\Phi = A \cdot V_C \cdot \sin\delta \quad (1)$$

where A is the age of the incoming oceanic crust, and the vertical descent rate is equal to the product of the convergence velocity [V_C] and the sine of the dip angle [δ]; Figure 1 [*Kirby et al.*, 1996; *Gorbatov and Kostoglodov*, 1997]. Equation (1) is proportional to the maximum depth reached by a given isotherm and therefore Φ, which is known as the thermal parameter, is a proxy for the thermal structure of the downgoing plate (i.e., fast subducting, old slabs [high-Φ] should be cooler than slowly subducting, young slabs [low-Φ] at equivalent depths). Recent geodynamic models confirm this relationship (Figure 2) [*Peacock*, 2003; *Syracuse et al.*, 2010; *van Keken et al.*, 2011] and are consistent with observed variations in temperature-dependent H_2O/LREE (light rare earth element) ratios in eruptive products from volcanic arcs with different Φ values [*Plank et al.*, 2009; *Cooper et al.*, 2012].

[3] Differences in slab thermal structure should exert considerable influence on the temperature-dependent chemical reactions occurring within descending slabs because mineral dehydration and breakdown reactions are expected to occur at shallower depths in slabs characterized by low-Φ compared to those characterized by higher Φ values (Figure 2) [*Schmidt and Poli*, 1998; *Peacock*, 2003; *Hacker et al.*, 2003; *Hacker*, 2008; *Syracuse et al.*, 2010]. Therefore, significant differences should exist between slab-derived components produced beneath arc segments characterized by different thermal parameters, and these differences should manifest in the chemical composition of magmas erupted at the surface.

[4] Arc magmas display elevated large ion lithophile (LILE) contents and negative Nb-Ta anomalies compared to primitive magmas from other tectonic settings (e.g., mid-ocean ridge basalts [MORB], back-arc basin basalts [BABB], ocean island basalts [OIB]) and these compositional attributes logically reflect slab contributions [e.g., *Gill*, 1981; *Plank and Langmuir*, 1988; *Sun and McDonough*, 1989; *Elliott*, 2003]. Ratios of LILE to LREE and high-field strength (HFSE) elements (e.g., Ba/La, K_2O/TiO_2) have long been used as proxies for slab contributions to arc magmas [e.g., *Kay*, 1978; *Gill*, 1981; *Leeman et al.*, 1990; *Stolper and Newman*, 1994; *Pearce and Peate*, 1995] because LILEs preferentially partition into the fluid phase during slab dehydration and into the melt phase during melting. However, the slab-derived component is considerably more complex than a single fluid composition and ranges in character from solute-poor aqueous fluids (>80% H_2O) at subsolidus temperatures to hydrous partial melts (<30% H_2O) of sediment and oceanic crust at higher temperatures [*Manning*, 2004; *Kessel et al.*, 2005; *Hermann and Spandler*, 2008]. Additionally, thermal gradients and lithologic differences within the slab itself should produce multiple fluids that are added to the overlying mantle wedge at any given depth [e.g., *Schmidt and Poli*, 1998; *Hacker*, 2008]. At sufficiently high pressures (>6 GPa), beyond the volcanic arc, these end-member slab components form a miscible compositional continuum, complicating traditional slab tracer ratios by mobilizing

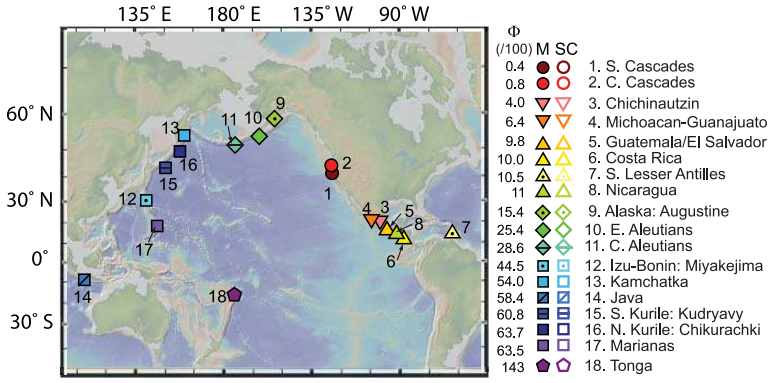

Figure 1. Map (from GeoMapApp) showing the locations of the arc segments examined here. Arc segments are labeled and color-coded from low slab thermal parameter (warm colors) to high (cool colors). Average Φ values are shown to the right along with symbols (M: magma, SC: subduction component).

HFSEs and other elements traditionally considered fluid immobile [*Manning*, 2004; *Kessel et al.*, 2005; *Hermann et al.*, 2006]. At lower pressures these two end-members may mix in varying proportions as they are added to the overlying mantle wedge [e.g., *Elliott*, 2003; *Eiler et al.*, 2005; *Le Voyer et al.*, 2010; *Martin et al.*, 2011].

[5] Measurements of dissolved volatiles (H_2O, S, Cl, CO_2) in submarine glasses and olivine-hosted melt inclusions permit direct comparison of magmatic volatile contents with trace element proxies [e.g., *Stolper and Newman*, 1994; *Cervantes and Wallace*, 2003; *Wade et al.*, 2006; *Portnyagin et al.*, 2007; *Johnson et al.*, 2009; *Ruscitto et al.*, 2010]. Importantly, volatile/trace element ratios constrained by experimental work have given rise to provisional slab-fluid geothermometers that permit robust comparisons between subduction zones characterized by different thermal regimes [*Plank et al.*, 2009]. In a companion paper [*Cooper et al.*, 2012], we modified the H_2O/Ce slab fluid geothermometer of *Plank et al.* [2009] to include pressure effects, and we applied it to H_2O/Ce data from a number of arcs to investigate how predicted slab surface temperatures compare to the geodynamic model temperatures of *Syracuse et al.* [2010]. In this paper, we expand on that study, which focused on H_2O/Ce in melts and slab fluids, by independently compiling a global data set of primitive arc magma compositions (in equilibrium with mantle olivine) for 100 volcanic centers encompassing the global range in slab thermal parameter (Figure 1 and Table 1). We use this global data set to examine the relationships between volatiles, slab tracers, and computed subduction component compositions with variations in the slab thermal structure and depth beneath the arc. We also examine the magmatic volatile fluxes for three well studied arcs spanning a large range in slab thermal parameter to look for variations in volatile recycling efficiency that might relate to temperature of the slab. Our results provide strong evidence for the active supply of subduction-related components from the slab beneath volcanic arcs and show that calculated subduction component compositions have higher trace element to H_2O ratios in arcs with hotter slabs (lower Φ).

2. Data and Methods

[6] Volcanic centers were grouped into arc segments using the physical parameters compiled in the

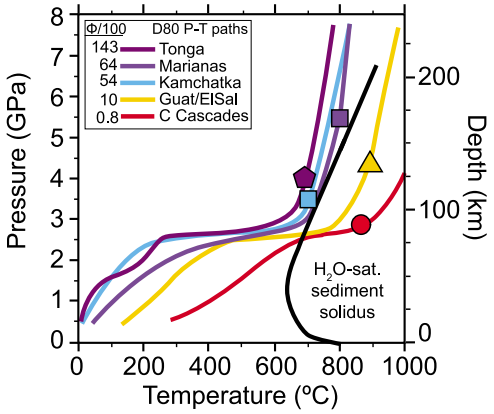

Figure 2. Pressure-temperature paths of model slab surfaces for five arc segments spanning the global range in slab thermal parameter (paths correspond to D80 models of *Syracuse et al.* [2010]). Average depth to the slab surface beneath each volcanic front is indicated by the symbol (as in Figure 1) along each P-T path. The black solid line represents the H_2O-saturated solidus for subducting sediment based on experiments by *Hermann and Spandler* [2008].

Table 1 (Sample). Primitive Magma Compositions[a] [The full Table 1 is available in the HTML version of this article]

Arc Segment	Volcano/Vent	h[b] (km)	Φ (/100, km)	H_2O (wt.%)	1s.d.[c]	S (wt.%)		Cl (wt.%)		B (ppm)		Ba (ppm)		La (ppm)		Nb (ppm)		Ce (ppm)	
Southern Cascades			0.4	2.8	±1.2	0.14	±0.08	0.21	±0.07	11.3	±5.2	168	±124	10.6	±1.2	2.3	±1.1	30.8	±3.6
	Goosenest [6]	86		2.7	±0.1	n.d.		n.d.		n.d.		n.d.		n.d.		n.d.		n.d.	
	Copco [6]	89		1.3	±0.1	n.d.		n.d.		n.d.		n.d.		n.d.		n.d.		n.d.	
	Shasta PBA [51, 52]	90		4.0	±0.6	0.20	±0.01	0.26	±0.01	7.6	±5.4	81	±9	9.8	±0.3	1.5	±0.1	28.2	±1.9
	Shasta HMA [51, 52]	90		3.3	±0.5	0.08	±0.00	0.16	±0.00	15	±2.0	256	±15	11.5	±0.9	3.1	±0.1	33.3	±2.1
	Black Crater[d] [6]	*108*		*0.3*	*±0.1*	*n.d.*		*n.d.*		*n.d.*		*n.d.*		*n.d.*		*n.d.*		*n.d.*	
Central Cascades			0.8	2.3	±0.6	0.10	±0.03	0.05	±0.02			246	±79	10.5	±3.4	7.7	±2.5	26.5	±8.6
	Sand Mountain [53]	85		2.9	±0.2	0.15	±0.05	0.09	±0.03	n.d.		356	±8	18.3	±0.1	12.4	±2.3	43.0	±0.4
	Twin Craters [48]	86		1.6	±0.1	0.11	±0.02	0.03	±0.01	n.d.		318	±26	11.5	±1.4	6.3	±0.6	32.7	±3.5
	Island Fissure [48]	88		2.3	±0.2	0.11	±0.01	0.04	±0.00	n.d.		413	±40	14.9	±0.8	12.2	±0.9	39.5	±3.1
	Four-in-One [53]	88		2.6	±0.4	0.08	±0.00	0.07	±0.00	n.d.		216	-	10.2	-	6.1	-	20.5	-
	Collier [48]	89		3.4	±0.4	0.07	±0.01	0.06	±0.01	n.d.		199	±28	7.9	±2.6	6.8	±3.2	18.7	±4.3
	Yapoah [48, 53]	89		2.6	±0.3	0.08	±0.02	0.08	±0.02	n.d.		230	±40	8.5	±1.0	5.7	±1.6	21.3	±2.4
	Blue Lake [48]	89		3.0	±0.3	0.13	±0.03	0.06	±0.01	n.d.		210	±38	6.7	±1.8	4.6	±1.3	17.4	±3.6
	Garrison Butte [48]	96		1.4	±0.2	0.11	±0.01	0.05	±0.02	n.d.		189	±9	10.5	±1.0	8.3	±0.5	28.1	±1.7
	CC021[e] [32, 48]	92		2.3	±0.3	0.09	±0.00	0.06	±0.00	n.d.		195	±7	7.9	±0.3	6.9	±0.3	20.1	±0.8
	BC021[e] [32, 48]	93		1.6	±0.6	0.09	±0.00	0.03	±0.00	n.d.		185	±7	9.6	±0.4	8.4	±0.3	24.9	±1.0
	DB042[e] [32, 48]	94		1.9	±0.4	0.08	±0.01	0.03	±0.00	n.d.		190	±5	9.2	±0.2	7.0	±0.2	24.9	±0.5
	BR022[e] [32, 48]	*105*		*2.2*	*±0.1*	*0.08*	*±0.00*	*0.03*	*±0.00*	*n.d.*		*175*	*±14*	*7.0*	*±0.6*	*7.3*	*±0.4*	*19.6*	*±1.5*
	KWB03[e] [32, 48]	*106*		*2.5*	*±0.3*	*0.09*	*±0.00*	*0.04*	*±0.00*	*n.d.*		*285*	*±20*	*8.8*	*±0.7*	*5.9*	*±0.3*	*23.4*	*±2.0*
	BB031[e] [32, 48]	*107*		*1.6*	*±0.3*	*0.10*	*±0.01*	*0.03*	*±0.00*	*n.d.*		*255*	*±57*	*9.2*	*±0.1*	*6.9*	*±0.9*	*25.4*	*±0.1*
	LTB022[e] [32, 48]	*107*		*2.2*	*±0.1*	*0.09*	*±0.00*	*0.03*	*±0.00*	*n.d.*		*236*	*±6*	*8.5*	*±0.3*	*8.0*	*±0.5*	*23.3*	*±0.7*
	AIC021[e] [32, 48]	*108*		*2.0*	*±0.2*	*0.11*	*±0.01*	*0.03*	*±0.00*	*n.d.*		*177*	*±7*	*7.5*	*±0.2*	*8.0*	*±0.1*	*21.3*	*±0.5*
	ELK021[e] [32, 48]	*111*		*1.6*	*±0.4*	*0.10*	*±0.01*	*0.03*	*±0.00*	*n.d.*		*312*	*±155*	*8.2*	*±1.3*	*6.4*	*±1.0*	*20.4*	*±3.4*
	TB021[e] [32, 48]	*111*		*2.2*	*±0.5*	*0.09*	*±0.00*	*0.05*	*±0.00*	*n.d.*		*248*	*±16*	*8.4*	*±0.4*	*6.4*	*±0.7*	*22.0*	*±1.4*
	SIC021[e] [32, 48]	*114*		*2.2*	*±0.2*	*0.08*	*±0.01*	*0.03*	*±0.00*	*n.d.*		*124*	*±7*	*4.8*	*±0.4*	*4.6*	*±0.5*	*14.7*	*±1.2*

[a]References: 1. *Marsh* [1982]; 2. *Nye and Reid* [1986]; 3. *Hawkins et al.* [1990]; 4. *Romick et al.* [1990]; 5. *Miller et al.* [1992]; 6. *Sisson and Layne* [1993]; 7. *Leeman et al.* [1996]; 8. *Stolper and Newman* [1994]; 9. *Gribble et al.* [1996]; 10. *Johnson et al.* [1996]; 11. *Elliott et al.* [1997]; 12. *Roggensack et al.* [1997]; 13. *Sisson and Bronto* [1998]; 14. *Eiler et al.* [2000]; 15. *Newman et al.* [2000]; 16. *Roggensack* [2001]; 17. *Haase et al.* [2002]; 18. *Kent and Elliott* [2002]; 19. *Myers et al.* [2002]; 20. *Cervantes and Wallace* [2003]; 21. *George et al.* [2003]; 22. *Tolstykh et al.* [2003]; 23. *Walker et al.* [2003]; 24. *Jicha et al.* [2004]; 25. *Eiler et al.* [2005]; 26. *Gurenko et al.* [2005]; 27. *Kelley et al.* [2006]; 28. *Wade et al.* [2006]; 29. *Wysoczanski and Tani* [2006]; 30. *Singer et al.* [2007]; 31. *Benjamin et al.* [2007]; 32. *Portnyagin et al.* [2007]; 33. *Rowe et al.* [2007]; 34. *Bouvier et al.* [2008]; 35. *Sadofsky et al.* [2008]; 36. Shaw *et al.* [2008]; 37. *Auer et al.* [2009]; 38. *Bezos et al.* [2009]; 39. *Bolge et al.* [2009]; 40. *Johnson et al.* [2009]; 41. *Mangan et al.* [2009]; 42. *Roberge et al.* [2009]; 43. *Rowe et al.* [2009]; 44. *Bouvier et al.* [2010]; 45. *Cooper* [2010]; 46. *Cooper et al.* [2010]; 47. *Kelley et al.* [2010]; 48. *Ruscitto et al.* [2010]; 49. *Saito et al.* [2010]; 50. *Zimmer et al.* [2010]; 51. *Martin et al.* [2011]; 52. *Ruscitto et al.* [2011]; 53. D. M. Ruscitto, unpublished, 2011; 54. N. Vigouroux, unpublished, 2011.

[b]Distance from the top of the slab (h) are taken from *Syracuse and Abers* [2006] or have been calculated for other vents by first measuring the distance from the edifice to the trench, perpendicular to the strike of the trench (d_{meas}). To keep new measurements consistent with the *Syracuse et al.* [2010] models we calculated h by using the equation: $h = h_{avg} + (d_{meas} - d_{avg}) \cdot \tan(\delta)$; where h_{avg} and d_{avg} are the average distances to the top of slab and trench, respectively, for the arc segment and δ is the average slab dip angle taken from *Syracuse et al.* [2010].

[c]1 standard deviation (s.d.) reported for arc segment averages, 1 standard error (s.e.) reported for individual vents. Only analytical errors are reported for maximum H_2O contents. The errors reported for average S, Cl, and trace element contents reflect melt inclusion variability used to calculate the average. Uncertainties related to extents of crystallization, oxidation states, and Fe-Mg K_D values (described in text) are not included. A "-" sign indicates either no estimate is reported or only a single measurement was used.

[d]Vents in italics were not used to determine average arc segment values and are either too far behind the VF or are not subduction-related.

[e]Estimated H_2O contents for Central Cascades using relationships with TiO_2, Er, and Yb contents after *Ruscitto et al.* [2010].

study by *Syracuse and Abers* [2006] and *Syracuse et al.* [2010], along with two additional segments for the Southern Cascades (Shasta region) and the Michoacán-Guanajuato Volcanic Field (MGVF) in Mexico (Table 1). The Φ parameter (equation (1)) for the Southern Cascades segment was calculated using δ = 19.8° (same as Central Cascades), V_C = 21 km/Ma [*Miller et al.*, 2001], and A = 6 Ma [*Wilson*, 2002]. The slower convergence rate and younger age of the incoming plate result in a lower Φ value calculated for the Southern Cascades arc segment when compared to the Central Cascades segment (Φ ∼40 km instead of 80 km). Subduction parameters for the MGVF segment were based on the geodynamic model in the work of *Johnson et al.* [2009] (δ = 43°, V_C = 53 km/Ma, A = 17.6 Ma) and result in Φ ∼640 km, higher than that calculated for the Chichinautzin Volcanic Field (CVF) arc segment in eastern Mexico (∼400 km).

[7] Primitive magma compositions (i.e., in equilibrium with $Fo_{90–91}$ olivine) were calculated from basaltic to basaltic andesite melt inclusion (predominantly olivine-hosted) and whole rock data for each volcanic edifice. The volcanic vents, selected compositional data for the primitive magmas (including initial volatile estimates), and estimated amounts of olivine addition required for mantle equilibration are listed in Table 1. We used olivine-hosted melt inclusion compositions that had been restored to equilibrium with their host crystals as reported in the original published data sources. Major and trace elements for primitive magma compositions from each volcano were determined by averaging the least evolved melt inclusions (i.e., highest MgO contents) and then incrementally adding equilibrium olivine (0.1 wt.%) until the melt composition was equilibrated with the mantle (e.g., Fo_{90}). This method assumes that crustal contamination has not significantly modified erupted compositions. This assumption may be appropriate as all of the data used have been pre-screened to include only the most mafic compositions. A complete description of the data treatment and sources is provided in Text S1 in the auxiliary material, and the full primitive magma compositions calculated for each volcano are provided in Table S1.[1]

[8] We used the thermobarometer of *Lee et al.* [2009] to test whether our calculated compositions were consistent with equilibration in the sub-arc mantle wedge (Figure 3 and Table S1). All but one of the primitive melt compositions are consistent with final mantle equilibration occurring at or below the base of the crust (represented by the Moho and shown for each arc segment in Figure 3) at temperatures near or slightly less than the dry solidus for a fertile peridotite. The P-T conditions computed for the primitive high-Mg composition from Mt. Shasta, Southern Cascades, are inconsistent with final equilibration in the mantle wedge (Figure 3a); sub-Moho equilibration for this composition would require more than 10–14 wt.% H_2O [*Parman and Grove*, 2004; *Ruscitto et al.*, 2011]. The points shown in Figure 3 represent the various P-T conditions at which melts, formed in the hottest part of the mantle wedge (e.g., 1350°C and ∼4 GPa), have re-equilibrated with peridotite at cooler, shallower conditions upon ascent (shown schematically by the thick blue arrow in Figure 3e). BABB compositions (x's in Figure 3e) indicate final equilibration with the mantle at slightly hotter temperatures than the arc magmas, above the fertile dry peridotite solidus, and our results are consistent with those of *Kelley et al.* [2010] using similar methods.

3. Results

3.1. Global Arc Magma Variability

[9] Figure 4 shows volatile abundances of the primitive magmas (e.g., corrected to $Fo_{90–91}$) relative to vent distance above the subducting slab (h, km) beneath each volcano. Considerable variability in the volatile contents from the global arc data set is apparent, and some may be attributed to either pre-entrapment degassing or post-entrapment diffusive H loss from the melt inclusions. Most of the observed variability, however, is likely real as all of the volatile estimates are based on least-degassed melt inclusions from each volcano. Dissolved volatiles in magmas erupted farther behind the volcanic front (VF) (or at greater h, assuming similar dip angles) do not show the steady decrease that might be expected to result from diminishing slab contributions behind the arc. Almost all of the arc magmas (both at and behind the VF), as well as BABBs, contain higher H_2O, B and Cl contents than are typically found in MORB and OIB (Figures 4a, 4b, and 4c [*Wallace*, 2005]). There are, however, MORB and OIB-like magmas erupted within some arcs, and these tend to be relatively volatile-poor, consistent with a likely origin by decompression rather than flux melting [e.g., *Grove et al.*, 2002]. Both arc magmas and BABBs display more overlap with MORB values at the low end of the S concentration range (Figure 4d). This is probably because

[1] Auxiliary materials are available in the HTML. doi:10.1029/2011GC003887.

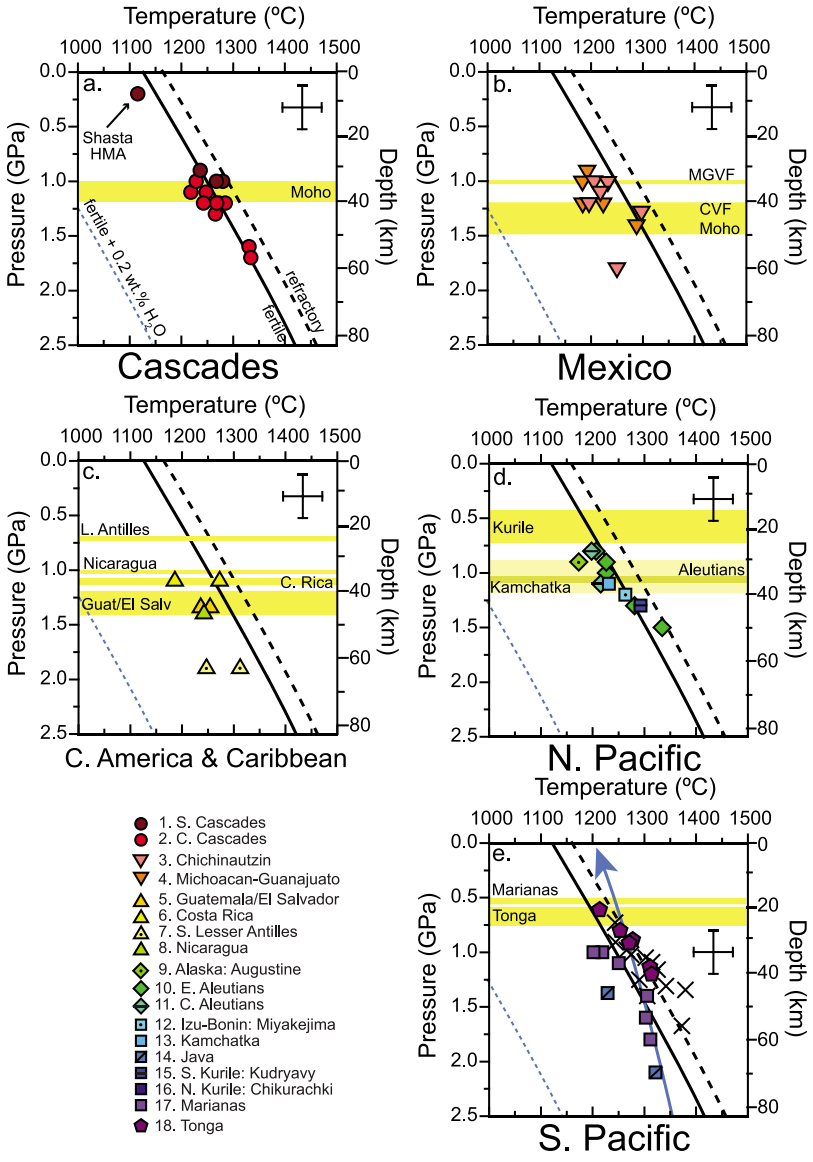

Figure 3. Final mantle-melt equilibration conditions for parental arc magmas calculated using the geothermobarometer of *Lee et al.* [2009]. Arc symbols are the same as in Figure 1 along with 'X' showing back-arc basin basalt (BABBs) glasses from the Marianas Trough, East Scotia Ridge, Lau Basin, Manus Basin, Ngatoro Basin, and Havre Trough [*Hawkins et al.*, 1990; *Stolper and Newman*, 1994; *Gribble et al.*, 1996; *Newman et al.*, 2000; *Haase et al.*, 2002; *Kelley et al.*, 2006; *Wysoczanski and Tani*, 2006; *Bezos et al.*, 2009]. Plots have been split up into different regions for clarity. Thick solid and dashed lines represent the anhydrous solidi for fertile [*Hirschmann*, 2000] and refractory [*Wasylenki et al.*, 2003] mantle compositions, respectively. Thin blue dashed line represents a hydrated mantle solidus (0.2 wt.% H_2O) after *Kelley et al.* [2010]. Error bars (~2 s.d.) for pressure and temperature estimates are 0.2 GPa and 38°C [*Lee et al.*, 2009]. Blue arrow in Figure 3e schematically illustrates ascent path for a hydrous magma produced at T = 1350°C. Labeled yellow bands mark the approximate locations of the Moho beneath each arc segment: Cascades (35–40 km [*Hildreth*, 2007]), MGVF and CVF (35 km and 45–50 km, respectively [*Wallace and Carmichael*, 1999, and references therein]), Central America (Guat/El Salv: 40–48 km, Nicaragua: 35 km, Costa Rica: 35–38 km [*Carr et al.*, 2003]), L. Antilles (24 km [*Kopp et al.*, 2011]), Aleutians (darker line in Figure 3d, 35–37 km [*Shillington et al.*, 2004]), Kamchatka (30–40 km [*Levin et al.*, 2002]), Kurile (15–25 km [*Dreyer et al.*, 2010, and references therein]), Tonga (20–25 km [*Crawford et al.*, 2003; *Cooper et al.*, 2010]), Marianas (17–20 km [*Takahashi et al.*, 2007]).

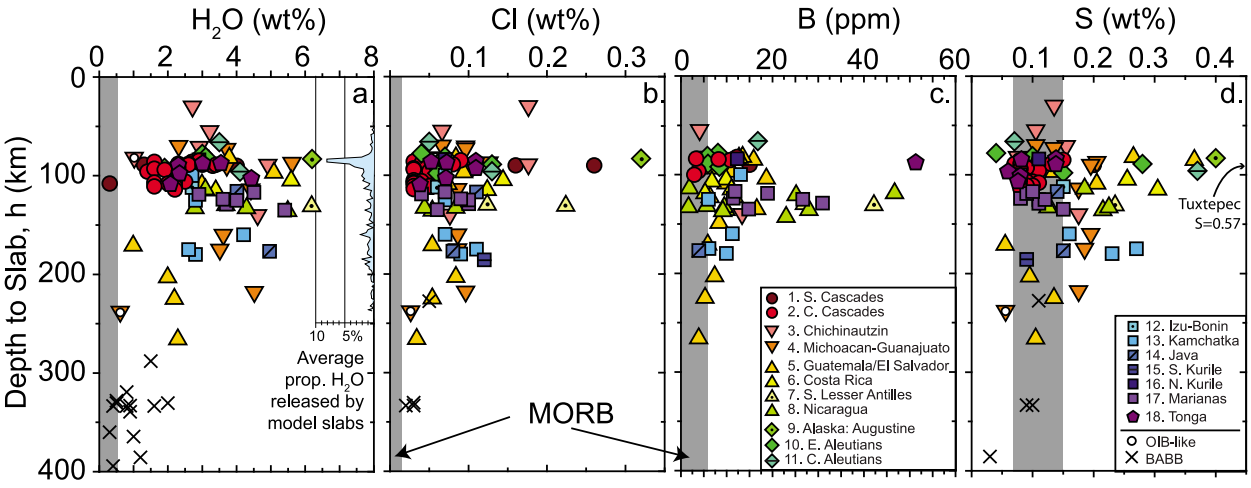

Figure 4. Initial H_2O, Cl, B, and S contents of primitive magmas for individual volcanoes plotted against depth to the slab (h, km). Symbols for arc volcanoes are the same as in Figure 1, with the addition of a white 'o' inside ocean island basalt-like (OIB-like) samples from Mexico [*Cervantes and Wallace*, 2003; *Johnson et al.*, 2009]. Back-arc basin basalt glasses (BABB) from the Marianas Trough, East Scotia Ridge, Lau Basin, Manus Basin, Ngatoro Basin, and Havre Trough are shown as 'X's. The shaded field in the H_2O, Cl, and S panels represents the range in N-MORB [*Wallace*, 2005]; in Figure 4c it represents the MORB range [*Ryan and Langmuir*, 1993]. Inset along the right of the H_2O panel shows the average proportion of H_2O released by slabs at a given depth modeled by *van Keken et al.* [2011].

the low fo_2 end of the arc magma spectrum overlaps with MORB [e.g., *Kelley and Cottrell*, 2009], under which conditions S contents in melts are limited by immiscible sulfide liquid saturation [*Wallace and Carmichael*, 1992]. Magmas containing the highest volatile contents erupt from vents situated ~90–120 km above subducting slabs (Figure 4). These depths are consistent with those predicted by geodynamic models, in which the greatest amounts of slab-derived fluids are released during dehydration reactions occurring just below the slab-mantle coupling depth (Figure 4a) [*van Keken et al.*, 2011].

[10] Elevated volatile contents in arc magmas erupted from vents located behind VFs, where there is a greater depth to the slab (i.e., $h > 100$ km), may indicate: (1) downdip migration of hydrated mantle resulting from wedge corner flow [e.g., *Grove et al.*, 2009]; (2) continued, deeper slab dehydration, albeit with a lower flux at greater slab depths; and/or (3) release of fluids from serpentinite in the mantle of the downgoing slab. Some of the volatile-rich samples erupted from vents located behind the VF are from regions of the Trans-Mexican Volcanic Belt that currently are (CVF) or were (MGVF) influenced by flat-slab subduction (note MGVF La Loma at 4.6 wt.% H_2O and 220 km in Figure 4a), which likely complicates fluid-release versus depth systematics in the slab. Apart from this complication, the overall data trends support the contention that the majority of volatiles in mafic arc magmas are derived from the subducting oceanic plate. We also note that magmatic volatile contents at the VF are not uniformly higher than those in back-arc regions (higher h), where contributions from the slab are expected to be diminished [e.g., *Schmidt and Poli*, 1998; *Kelley et al.*, 2006; *Bezos et al.*, 2009]. Instead VF magmas display considerable scatter but extend to higher average values (Figure 4).

[11] Primary volatile contents for each magma composition are plotted against the slab thermal parameter characterizing each arc segment in Figure 5. There is considerable overlap in the H_2O, Cl, and S contents of primitive magmas across the full range of Φ values for the global data set. The highest volatile contents occur in arc segments characterized by intermediate Φ values (900–1500 km), although this may not be statistically significant. The global average H_2O content is 3.3 ± 1.2 wt.% (1 s.d.) for primitive magmas erupted within ~50 km of the volcanic front. The highest primary H_2O contents from our data set (>6.0 wt.%) come from Grenada (L. Antilles) and Augustine (Alaska); vents located in arc segments with Φ values of 1050 and 1540 km, respectively (Figure 5a). Segments characterized by the lowest Φ values (Cascades and CVF, Mexico) show considerable variability and, whereas the Cascades generally have lower H_2O contents (1.3–4 wt.%) than other arcs, mafic magmas in the CVF contain up to 5.0 wt.% H_2O. Thus, maximum H_2O contents in

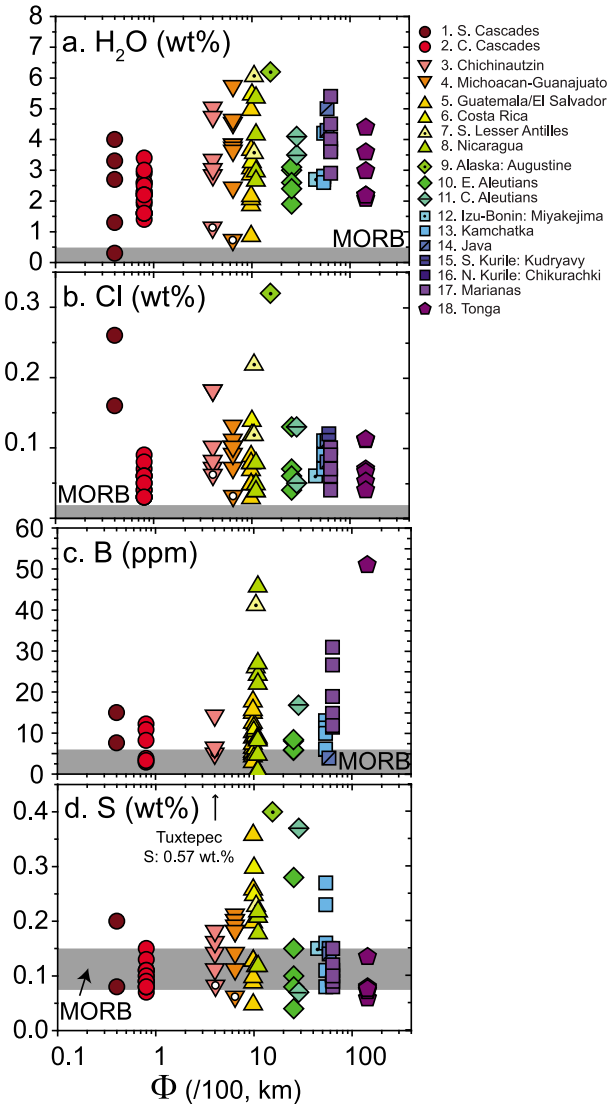

Figure 5. Initial H_2O, Cl, B, and S contents of primitive magmas for individual volcanoes plotted versus arc segment thermal parameter (Φ). The shaded field in each panel represents the range in MORB values (from Figure 4).

these 'warm slab' arc segments nearly encompass the entire range of H_2O contents in magmas from both the Tonga (2.4–4.4 wt.%) and Marianas (2.9–5.4 wt.%) arcs, both of which are at the extreme high-Φ end of the global arc spectrum. Variations in Cl and S concentrations with slab thermal parameter generally follow the same pattern observed for H_2O, with Cl patterns being somewhat more obscured by the Cl-rich high-Mg andesites from the Shasta Region in the Southern Cascades (Figures 5b and 5d) [*Ruscitto et al.*, 2011]. B contents generally increase with thermal parameter [e.g., *Leeman*, 1996], and the highest B contents are found in magma from the Tonga arc (Tofua; Figure 5c). In subsequent discussions, only arc magmas erupted within ~50 km of each VF are considered in order to avoid potential complications arising from the expected increasing influence of decompression melting in back-arc regions [e.g., *Sisson and Layne*, 1993; *Walker et al.*, 2003].

[12] Crude positive correlations (p-values for slopes are <0.02, meaning that the slopes are positive within >98% confidence interval) are observed on a global scale between magmatic H_2O contents and Cl, S, and B, although there is considerable scatter within the global data set (low r^2 values; Figures 6a–6c). Most primitive magmas have restricted H_2O/Cl ratios that are consistent with mixing between a MORB source mantle and seawater (3.5 wt.% NaCl equivalent [*Kent et al.*, 1999; *Johnson et al.*, 2009; *Ruscitto et al.*, 2010]) (Figure 6a). However, seawater B and S contents are much too low to reproduce the global arc magma array through such mixing, as are concentrations of all incompatible trace elements such as Ba (Figures 6b–6d). Barium, generally assumed to be a fluid-mobile element, does not correlate with H_2O, but there may be a broad increase in Ba/H_2O ratios from arcs with higher Φ (cooler) slabs toward those with lower Φ (warmer) slabs (Figure 6d).

[13] Although Ba and H_2O contents of the primitive magmas are not correlated, ratios of volatiles and trace elements of similar mineral-melt compatibility in the mantle (e.g., H_2O/Ce [*Dixon et al.*, 2002; *Hauri et al.*, 2006]) are elevated above MORB, BABB, and OIB and are positively correlated with ratios of traditional fluid-mobile/immobile slab tracers (e.g., Ba/La [*Elliott*, 2003]) (Figure 7a). Although the positive correlation illustrated in Figure 7a results primarily from the strong correlation between La and Ce in the denominators (r^2 ~ 0.99 [*Cooper et al.*, 2012]), similar positive correlations are observed between H_2O/Ce and Ba/Nb, Ba/Th and (to a lesser extent) Ba/Zr. H_2O/Ce ratios also positively correlate with Cl/Nb and B/La (Figures 7b and 7c) and negatively correlate with La/Sm (not shown). Some of the ratios presented in Figure 7 vary over several orders of magnitude, and therefore all correlations were tested using the robust Kendall-Theil method in order to reduce the influence of extreme values [*Helsel and Hirsch*, 2002]. Importantly, a second trend is embedded within the H_2O/Ce correlations with Cl/Nb and B/La (and to a lesser extent Ba/La) indicating that magmas originating in higher Φ subduction zones (e.g., Marianas, Tonga, Kamchatka; cooler colored

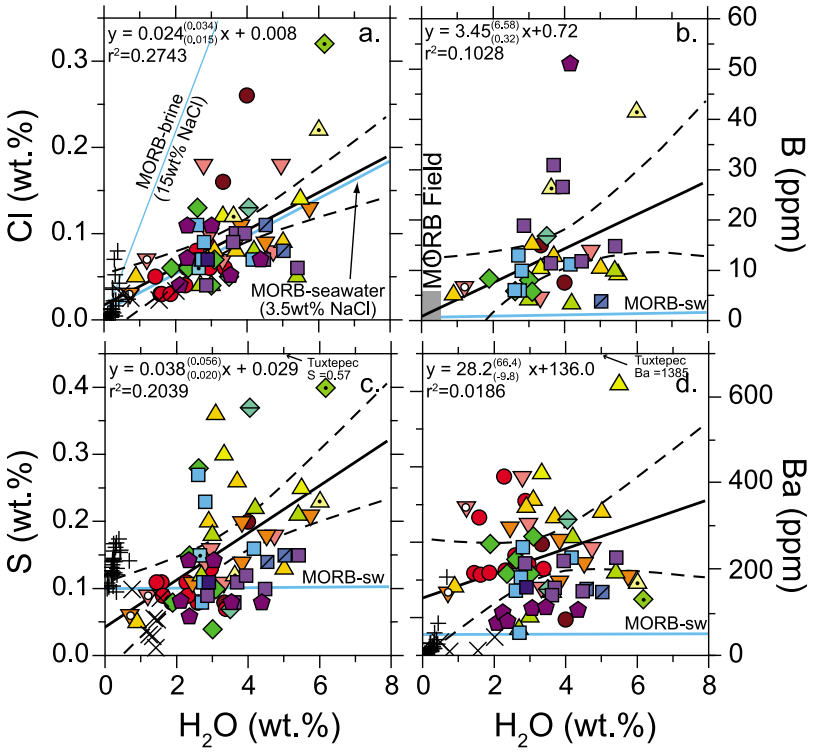

Figure 6. Bivariate plots of H_2O with Cl, B, S, and Ba contents of primitive magmas; arc, BABB, and OIB-like symbols as in Figures 1 and 4. Also shown are MORB glasses '+' from the East Pacific Rise [*Le Roux et al.*, 2006]. Thick solid and enveloping dashed lines correspond to the best fit linear regressions and 95% confidence intervals, respectively (equations and r^2 values in upper left of each panel; superscript and subscript denote upper and lower 95% confidence limits for slopes in each equation). (a) Light blue lines in this panel represent mixing between a MORB source (0.01 wt.% H_2O, 0.01 wt.% Cl, 0.1 wt.% S, 1.3 ppm B and 50 ppm Ba) and seawater (3.5 wt.% NaCl equivalent with 0.09 wt.% S, 4.5 ppm B, and 0.01 ppm Ba) or a concentrated brine (15 wt.% NaCl equivalent). (b, c, d) MORB-seawater mixing lines are also shown in these panels. MORB field shown in Figure 6b encompasses the range in H_2O contents from *Le Roux et al.* [2006] and the B contents from *Ryan and Langmuir* [1993].

symbols) tend to have higher ratios than magmas from lower Φ settings (e.g., Central Cascades, Chichinautzin, Mexico; warmer colored symbols), although this is somewhat obscured by regional variability that is most evident in magmas from Central America (Figure 7; see Section 3.2). Back-arc magmas from the Eastern Lau Spreading Center and the Mariana Trough are also consistent with Cl/Nb patterns observed for magmas generated beneath the VF (Figure 7b). MORB ratios from the East Pacific Rise (as well as OIB-like melts from Mexico: Hoya Alvarez and Xitle) are shown for comparison to highlight differences between magmas directly and not directly related to subduction.

3.2. Regional and Local Geochemical Overprinting

[14] The emphasis of this study is on global geochemical variations among volcanic arcs characterized by different Φ values, however, we recognize that regional/local variability can be considerable and obscure global trends. The geochemistry of arc magmas from Central America is particularly diverse, and the ranges in H_2O/Ce, Ba/La, and B/La ratios for this arc nearly encompass the global range for arc magmas compiled here (Figures 7 and 8). At first glance, this regional diversity is particularly troubling for correlations between H_2O/Ce and expected slab surface temperatures at a given depth (Section 4.1). Slab thermal parameters are largely similar between the Guatemala/El Salvador (Φ = 980 km), Costa Rica (1000 km), and Nicaragua (1100 km) arc segments and therefore these segments might be expected to have similar slab surface temperatures beneath the arc front (Section 4.1, Table 1) [*Plank et al.*, 2009; *Cooper et al.*, 2012]. Upon closer inspection however, most of the Central American magmas fall within a relatively restricted range in H_2O/Ce (1500–4000), comparable to the ranges found in other arcs, whereas Irazu and Cerro Negro define the extremes at ~780 and

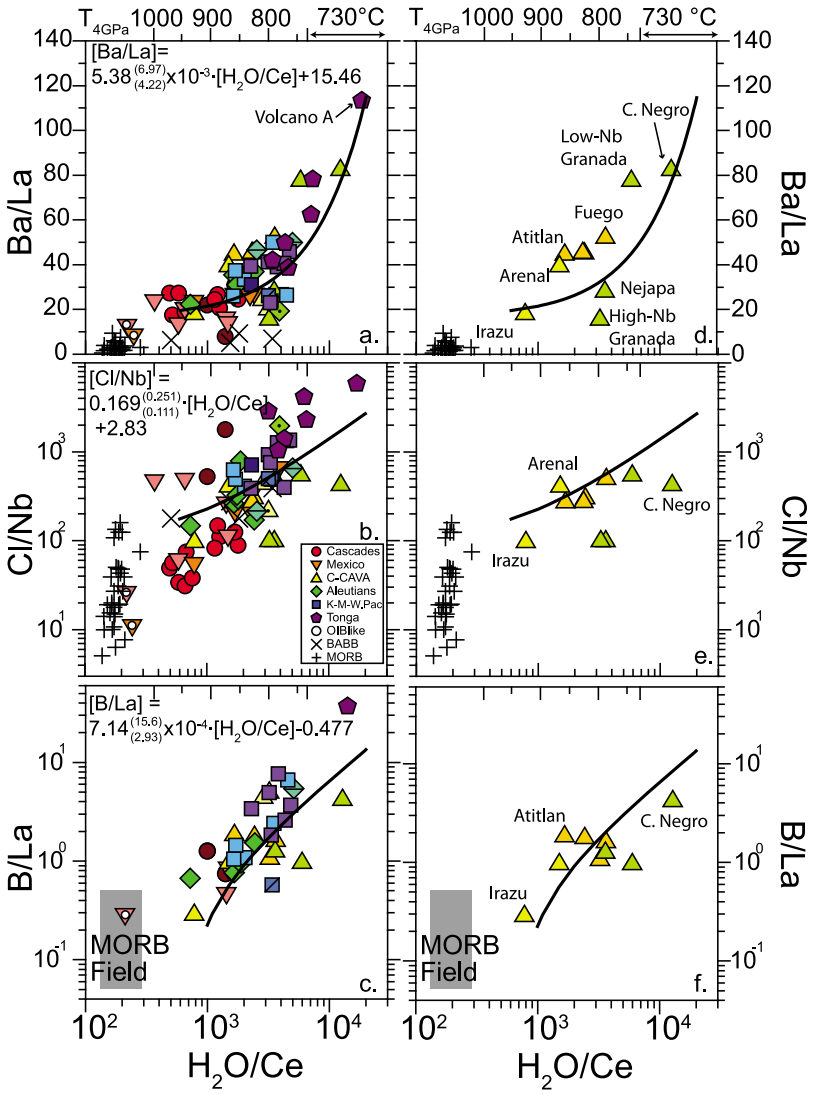

Figure 7. H_2O/Ce plotted against (a) Ba/La, (b) Cl/Nb, and (c) B/La for primitive magma compositions (symbols as in Figures 1 and 4). Legend is simplified for clarity: Cascades = Central and Southern Cascades; Mexico = MGVF and CVF; C-CAVA (Caribbean and Central American Volcanic Arcs) = Guatemala/El Salvador, Nicaragua, Costa Rica, and Southern Lesser Antilles; Aleutians = Alaska, Eastern and Central Aleutians; K-M-W.Pac (Kamchatka, Marianas, Western Pacific): Kamchatka, Marianas, Java, Kurile, Izu-Bonin. MORB glasses (from Figure 5), and BABB glasses are also shown. The spread in Cl/Nb contents of the MORB glasses illustrate seawater contamination to higher arc-like (>100) values. Thick lines through data are calculated using the robust Kendall-Thiel line [*Helsel and Hirsch*, 2002] through arc front magmas only (equations with confidence intervals of slopes are shown in each panel). Top axis corresponds to temperatures of slab fluids calculated from the provisional H_2O/Ce slab fluid geothermometer of *Plank et al.* [2009] at 3.5–4.5 GPa (equation (2) in text). (d, e, f) These panels shown to the right highlight the regional variability of the Central American primitive magmas as discussed in the text.

~12,850, respectively. The high H_2O/Ce ratios of Nicaraguan magmas may reflect contributions from fluids that have formed after exhaustion of LREE-bearing phases (allanite/monazite) in the subducting sediment during progressive slab dehydration attributed to either: (1) an excess supply of H_2O-rich fluids being fluxed through the slab during the breakdown of serpentine within the subducting lithospheric mantle [*Ranero et al.*, 2003; *Eiler et al.*, 2005; *Ivandic et al.*, 2008]; or (2) accelerated allanite/monazite exhaustion with the addition of less external H_2O resulting from the LREE-poor carbonate-dominated sediment overlying the Nicaragua slab [*Plank et al.*, 2002]. The lower magmatic H_2O/Ce ratio of Irazu is curious but may be attributed to the addition of locally REE-enriched sediment or slab-edge effects [see *Cooper et al.*, 2012].

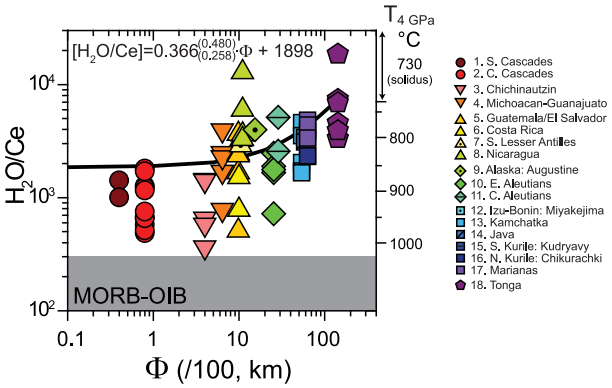

Figure 8. H_2O/Ce ratios of primitive arc-front magmas as a function of slab thermal parameter (Φ). Symbols as in Figure 1. Temperatures corresponding to the H_2O/Ce geothermometer at 3.5–4.5 GPa (equation (2) in text) are shown on the right-hand axis. The shaded region highlights the range in H_2O/Ce ratios found in mid-ocean ridge basalts (MORB) and ocean-island basalts (OIB). The thick black curve shows the Kendall-Thiel line and the corresponding equation is given in the upper left (along with the upper and lower confidence limits of the slope).

[15] Regional variability observed in other Central American trace element ratios, particularly in Ba/La (Figures 7a and 7d) and (to a lesser extent) B/La (Figures 7c and 7f) likely reflect variability of the incoming sediment package, which is both enriched in biogenic barite as a result of high biological productivity and depleted in LREE due to the carbonate-dominated lithology [*Plank and Langmuir*, 1993, 1998; *Plank et al.*, 2002]. We also point out that Central American Cl/Nb ratios fall within a relatively restricted range, comparable to the variation found in other arcs (Figures 7b and 7c). Thus, while Central America may represent an extreme case in terms of regional variability, other arcs also likely have regional variability (albeit to a lesser extent) in the composition of the downgoing slab and the mantle wedge. In summary, while there is an overall global relationship between Φ and arc magma geochemistry, regional variables may dominate in some regions.

4. Discussion

4.1. Slab-Fluid Geothermometry

[16] Recent work by *Plank et al.* [2009] combining experimental studies on fluids and melts from the subducted slab with accessory phase solubility determinations has yielded a provisional slab-fluid geothermometer:

$$H_2O/Ce = 2 \times 10^7 e^{-0.0109T} \quad (2)$$

The thermometer takes advantage of the large-scale (~3–4 orders of magnitude) variation in H_2O/Ce ratios (Ce as a proxy for light rare earth element concentrations) in allanite/monazite-saturated liquids at high pressure (3.5–4.5 GPa) over a modest temperature shift from ~600 to 1000°C. A companion paper [*Cooper et al.*, 2012] further modifies this thermometer by incorporating pressure dependence. Application of the geothermometer requires that the subduction component be saturated with a residual LREE-bearing accessory mineral (e.g., allanite or monazite) in order for the LREE contents of the fluid phase to reflect the calibrated relationship to temperature [*Plank et al.*, 2009]. This assumption is likely valid for both sediment and metabasalt given the wide stability fields for allanite and monazite [e.g., *Klimm et al.*, 2008; *Hermann and Rubatto*, 2009], and therefore measured H_2O/Ce ratios of primitive arc magmas potentially reflect the temperature of fluids (used here broadly to mean anything from aqueous fluid to hydrous melt to supercritical fluid) exiting the slab surface. We emphasize, however, that equation (2) is only applicable at temperatures above the water-saturated sediment solidus at 3.5–4.5 GPa (~730°C [*Hermann and Spandler*, 2008]) and extrapolation of the thermometer to subsolidus conditions would greatly underestimate slab fluid temperatures.

[17] Slab surface temperatures (SSTs) at 3.5–4.5 GPa, calculated using equation (2) and shown along the top axes in Figure 7, imply that (1) most slab-derived "fluids" are more accurately described as hydrous melts [see *Cooper et al.*, 2012], and (2) magmas generated in arcs with low-Φ (hotter) slabs are influenced by hotter fluids with more muted subduction-related signatures (i.e., lower ratios of Ba/La, Cl/Nb, B/La, closer to MORB/OIB values) compared to those generated beneath arcs with higher Φ (cooler) slabs. We test this observation further in Figure 8 and find a statistically significant (p-value < 0.05; within 95% confidence interval) positive correlation between H_2O/Ce ratios and Φ. Again, we used the robust Kendall-Theil method in order to reduce the influence of extreme H_2O/Ce values and the non-Gaussian distribution of Φ values. It may be suspected that the correlation in Figure 8 is spurious and that H_2O/Ce ratios are actually more sensitive to recycled Ce derived from variations in subducting sediment [e.g., *Plank and Langmuir*, 1998]; however, we find no correlation between magmatic H_2O/Ce and the Ce concentration of sediments being subducted at each arc. Therefore, we conclude that magmatic H_2O/Ce ratios largely reflect slab fluid temperatures at

depth. We emphasize, as shown in the Cooper et al. companion paper, that slab-fluid temperatures calculated using equation (2) are only applicable at 3.5–4.5 GPa and need to be adjusted along H_2O isopleths to the depth of the slab beneath any given volcano; for the purposes of this paper, however, all slab fluid temperatures are calculated at 4 GPa. Additionally, the H_2O/Ce ratios of the primitive magmas likely reflect the average temperature of multiple fluids released over a range of depths rather than the fluid temperature at a single location along the descending slab. We note that many studies have inferred multiple slab contributions to arc magmas involving varied proportions of subducting sediment and altered oceanic crust [*Elliott et al.*, 1997; *Eiler et al.*, 2005], and there is the additional possibility of both modern and ancient subduction components [*Borg et al.*, 2002; *Martin et al.*, 2011]. The slab components discussed in this work, however, represent the average 'non-mantle wedge' contribution to the magmas in each arc. Distinguishing the relative contributions of various sources beneath each arc requires detailed examination of trace element and isotopic data and is largely beyond the scope of this study.

[18] The shaded region in Figure 8 shows H_2O/Ce ratios of mantle-derived magmas not affected by subduction processes (200 ± 100 [*Dixon et al.*, 2002]). The fact that the provisional slab-fluid thermometer yields finite temperatures of ~1020–1120°C for these ratios even though no subduction component is involved suggests an alternative interpretation for the global arc H_2O/Ce variations. The apparent trends in Figures 6, 7, and 8 could potentially result from variable mixing between a MORB mantle source and a single, high-H_2O/Ce slab-derived component [e.g., *Stolper and Newman*, 1994; *Reiners et al.*, 2000; *Bezos et al.*, 2009] rather than from slab-temperature-dependent variations in H_2O/Ce. This alternative explanation may not be important in high-Φ arcs, where the very high H_2O/Ce of the subduction components is expected to swamp out any mantle signature, but it could be important in lower Φ arcs and in back-arc regions, where slab contributions to the mantle may be diminished after shallower dehydration (forearc or sub-arc, respectively) (e.g., Central Cascades, Chichinautzin, Mexico; Figures 1, 2, 6, and 7). Therefore, the H_2O/Ce ratios of the computed subduction fluid(s), rather than those from the magmas (melt inclusions), must be examined in order to distinguish between these two competing hypotheses.

4.2. Subduction Components

4.2.1. Modeling Mantle Melting and Subduction Component Addition

[19] Subduction components (SC) were calculated for the primitive magma compositions in Table 1 using the method outlined in the study by *Portnyagin et al.* [2007] (Table 2) by first assuming a starting mantle composition. The HFSE contents of the primitive melts are assumed to reflect only mantle melting, with negligible contributions of these elements coming from the subducting slab. The amount of previous melt extraction (*PME*, simulating prior mantle melting) and the degree of melting (F) required to produce a given primitive melt are then constrained by minimizing the misfit between the actual and model HFSE melt contents. This approach was slightly modified from *Portnyagin et al.* [2007] in that we determined average degrees of modal batch melting using only TiO_2, Dy, Er, Gd, Yb, and Y (excluding Nb and Zr) because these elements are not significantly mobilized in high pressure slab-derived fluids, even at temperatures of ~1000°C [*Kessel et al.*, 2005]. Using the *PME* and F values obtained from the HFSEs, the subduction-modified mantle wedge source composition can be reconstructed for all of the incompatible elements in the primitive magma. The differences between the *PME* mantle source and the subduction modified source reflect the contributions to the mantle wedge from the slab. The amounts of each element added to the mantle wedge are then calculated and normalized to 100% to yield a SC composition for each primitive magma. This approach differs slightly from that presented in the Cooper et al. companion paper, in which H_2O/Ce ratios of the SCs were estimated by extrapolating linear mixing lines between Nb/Ce ratios of assumed mantle sources and primitive magmas back to Nb/Ce of ~0.04. Their calculations yield comparable results to those presented here because of the similar compatibilities for H_2O and Ce during mantle melting. While a detailed discussion regarding hydrous melting in the sub-arc mantle is beyond the scope of this paper, we present the relationships between calculated degrees of melting and H_2O contents of primitive magmas and their inferred mantle sources that result from the SC calculations described above in Text S2.

[20] Ratios of H_2O/Ce, Cl/Nb, B/La, and Ba/La in the SCs are plotted in Figure 9. Relative uncertainties (1 s.e.) for SC H_2O/Ce and Ba/La are estimated to be ~13% and 11%, respectively (see Text S2 for

Table 2 (Sample). Calculated Subduction Components[a] [The full Table 2 is available in the HTML version of this article]

Volcano/Vent	Ba (ppm)	U (ppm)	Th (ppm)	K_2O (wt%)	Cl (ppm)	Nb (ppm)	La (ppm)	Rb (ppm)	H_2O (wt%)	Ce (ppm)	Sr (ppm)	Nd (ppm)	Na_2O (wt%)	Zr (ppm)	B (ppm)	Pb (ppm)	Sm (ppm)	Eu (ppm)	Σ Resid	PME (wt%)	F[b] (wt%)
Southern Cascades																					
Shasta PBA	1277	5.8	16.4	4.8	41679	23.6	153	77	65.5	440	16514	184	25.0	985	-	49	26	8.0	1.03	0.06	0.20
±1 s.e.	85	0.8	1.1	0.3	1789	1.3	7	8	1.6	22	710	9	1.3	49		4	2	0.6	0.13	0.00	0.01
Shasta HMA	3490	12.3	27.1	13.7	22150	42.1	154	279	47.7	445	11725	167	35.3	1188	-	92	25	7.3	0.92	0.06	0.14
	155	1.7	1.9	0.7	868	1.7	8	15	2.1	23	524	12	1.8	65		6	3	0.8	0.41	0.00	0.02
Central Cascades																					
Sand Mountain	5013	0.0	5.8	10.1	18087	0.0	216	69	47.7	495	16564	270	38.4	730	-	54	45	12.9	0.50	0.00	0.08
	480	1.3	2.6	1.1	2320	19.1	17	25	3.8	37	1247	20	3.1	133		10	8	1.2	0.09	0.00	0.01
Twin Craters	8496	0.0	1.2	11.2	11583	0.0	162	58	38.3	562	13831	316	47.2	145	-	72	60	23.7	0.38	0.00	0.08
	929	2.4	5.0	1.8	1377	0.0	26	46	3.8	57	1298	31	3.9	162		8	25	6.3	0.13	0.00	0.00
Island Fissure	8226	8.1	10.0	13.8	9071	35.2	209	235	41.5	574	11385	297	41.7	746	-	106	31	22.7	0.35	0.00	0.10
	543	2.3	4.1	1.2	607	18.9	14	27	2.5	35	675	21	1.8	123		24	5	2.3	0.11	0.00	0.00
Collier	3285	5.3	11.8	8.1	4523	37.1	113	128	56.0	238	6263	122	34.4	411	-	42	16	8.0	0.80	0.02	0.13
	269	0.7	1.2	0.8	369	25.2	20	12	2.7	34	483	24	2.3	225		3	5	1.7	0.27	0.00	0.02
Yapoah	3762	5.2	12.5	10.8	13888	15.7	123	144	42.4	282	7274	125	44.6	474	-	50	15	7.0	0.67	0.02	0.13
	343	1.1	2.2	1.3	1364	15.3	8	28	2.4	23	580	14	2.3	163		5	5	1.7	0.58	0.01	0.02
Blue Lake	3027	5.2	8.8	7.7	8412	23.1	95	113	44.3	238	7083	122	46.2	300	-	42	18	8.1	0.96	0.03	0.11
	227	1.0	1.0	0.4	715	9.5	10	11	2.0	21	246	12	1.8	117		3	3	1.1	0.41	0.01	0.03
Garrison Butte	5244	0.0	0.0	7.6	22937	0.0	185	21	44.0	544	14941	305	44.5	1121	-	91	43	27.4	0.14	0.00	0.09
	1014	1.7	1.8	2.2	8419	0.0	30	61	6.2	67	1997	41	4.9	573		21	15	5.3	0.07	0.00	0.00
Chichinautzin																					
Jumiltepec	5678	6.4	14.0	15.7	25321	53.4	269	-	39.5	592	8753	351	41.3	1607	0	-	59	44.5	0.84	0.05	0.19
Las Tetillas	2131	2.4	13.0	9.7	9995	26.3	104	-	45.7	259	3845	170	43.1	1284	65	-	35	17.1	0.67	0.01	0.23
Tepetlapa	3681	1.7	15.7	7.6	13766	103.0	217	-	45.2	599	8223	339	44.4	3412	0	-	72	60.6	0.82	0.00	0.09
Tuxtepec	13408	7.4	44.6	15.5	17791	39.2	560	-	50.6	1387	12573	846	29.3	1771	0	-	167	48.2	0.97	0.04	0.13
Popocatepetl	2317	4.3	20.4	8.6	7893	71.3	148	-	48.5	289	5462	212	41.1	1992	138	-	57	19.6	0.86	0.02	0.15
Michoacan-Guanajuato																					
San Juan	4782	2.8	8.8	7.4	12447	-	94	200	47.5	338	6200	191	42.6	801	-	67	35	0.0	0.22	0.00	0.11
Hungaro	3363	3.1	5.1	9.1	12522	-	98	114	50.8	214	5402	95	37.9	681	-	54	14	0.0	0.26	0.02	0.12
Jorullo	1472	1.0	3.1	5.7	11161	-	50	59	53.8	108	4041	74	38.8	547	-	33	14	0.0	0.28	0.11	0.07
Astillero	2023	1.6	4.1	6.9	13752	-	60	62	48.0	145	5051	84	43.0	369	-	33	20	0.0	0.17	0.03	0.13
Paricutin	2282	2.4	6.0	7.7	9815	-	65	80	50.7	159	5480	75	39.7	424	-	44	21	0.0	0.20	0.02	0.14

[a]Abbreviations: ΣResid is the sum of the residuals for the HFSE used to calculated *PME* (previous melt extraction) and *F* (the degree of melting). X_{SC} and $^{m}X_{H2O}$ are the required amounts of slab component added to and the initial H_2O contents of the mantle wedge, respectively, to produce the parent magmas with the *Portnyagin et al.* [2007] models.

[b]1 s.e. reported below *F* (wt.%) values for the Cascades are those determined by Monte Carlo simulations. The s.d. *F* estimates in the column to the right are those estimated by HFSE misfit to the models using the method of *Portnyagin et al.* [2007].

[c]Calculated SC lacks appreciable Na_2O, likely due to an overestimate in the mantle source.

more discussion of uncertainties). Uncertainties are considerably more variable (~2.5- > 1000%) for Cl/Nb and depend largely upon assumed mantle Nb contents. For example, the ultra-depleted mantle composition inferred to produce high-Mg magmas at Mt. Shasta (Southern Cascades segment) has ~0.0013 ppm Nb [*Grove et al.*, 2002] compared to the enriched mantle inferred to produce many of the Central Cascades magmas (0.69–1.13 ppm Nb). These differences require substantially more Nb to be added to the ultra-depleted source by the SC in order to produce a melt with Nb in the several ppm range, resulting in smaller Cl/Nb uncertainties. We point out that while the volatile and trace element ratios of the calculated SCs are typically 1.5–2.0 times higher than the ratios of the parental melts, differences in H_2O/Ce ratios do not greatly affect calculated slab surface temperatures because of the logarithmic nature of equation (2). In fact, most temperatures are in agreement to within 10%, and the greatest temperature deviations are observed for the higher Φ arcs where H_2O/Ce of the SC is expected to swamp out any mantle contributions to the melt. Therefore, despite some discrepancies, we conclude that the observed correlations of H_2O/Ce with Ba/La, Cl/Nb, and B/La do not result from mixing between a MORB source and a single volatile-rich fluid component, but instead reflect variations in the bulk SC compositions resulting from temperature differences in the slab beneath different arcs.

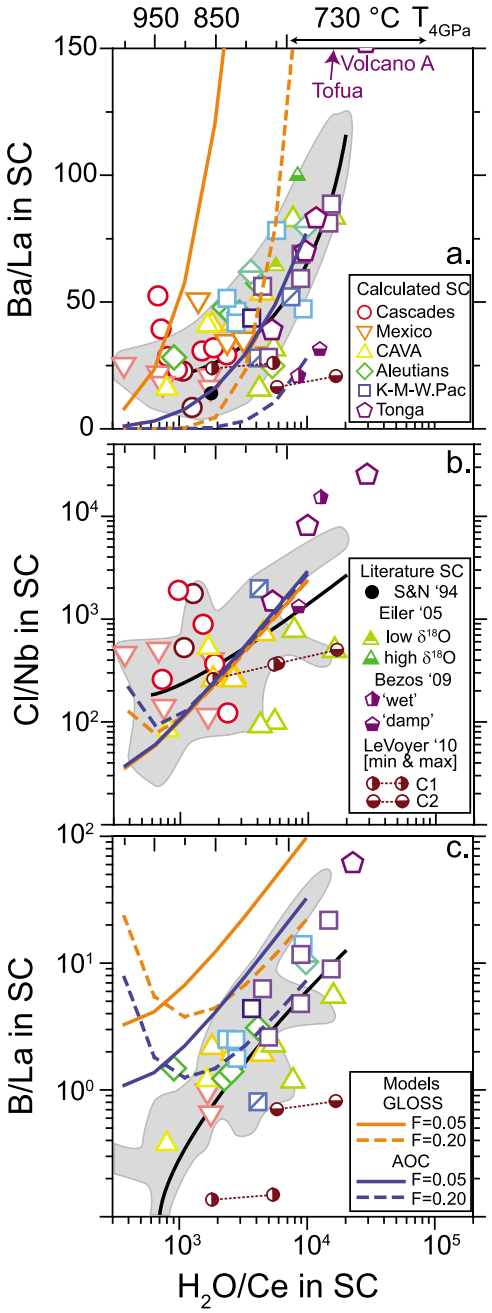

Figure 9. H_2O/Ce versus (a) Ba/La, (b) Cl/Nb, and (c) B/La ratios of calculated subduction components for the primitive magmas in Table 1. Open symbols (color and shape same as Figure 1) are used to emphasize that these are calculated SC components, not magmatic ratios. Estimated fluid compositions for Central America from *Eiler et al.* [2005], the Tonga back-arc from *Bezos et al.* [2009], the Marianas Trough from *Stolper and Newman* [1994], and the Shasta region from *Le Voyer et al.* [2010] (dotted lines connect minimum and maximum estimates for each component). Magmatic ratios (gray field) and Kendall-Thiel line (black line) from Figure 7 are shown for reference. Fractional melting models calculated using experimental fluid-melt partition coefficients at 4 GPa from *Kessel et al.* [2005], are shown for the altered oceanic crust ("Super" AOC [*Kelley et al.*, 2003]) and average global subducting sediment (GLOSS [*Plank and Langmuir*, 1998]) at *F* values of 0.05 (solid) and 0.20 (dashed). Top axis corresponds to temperatures of slab fluids calculated from the H_2O/Ce slab fluid geothermometer of *Plank et al.* [2009] at 3.5–4.5 GPa (equation (2) in text).

4.2.2. Nature of the Subduction Components

[21] Similarities between elemental ratios of the calculated SCs and the parent magmas (Figure 9) support our interpretation that magmas formed in low-Φ arc environments have been influenced by hotter slab-derived components than arcs characterized by higher Φ slabs. The positive correlations in Figure 7 (and to a lesser extent in Figure 9) suggest temperature-dependent variations in the composition of the subduction components released beneath different arc segments. We tested whether the thermo-chemical relationships in Figure 7 (and

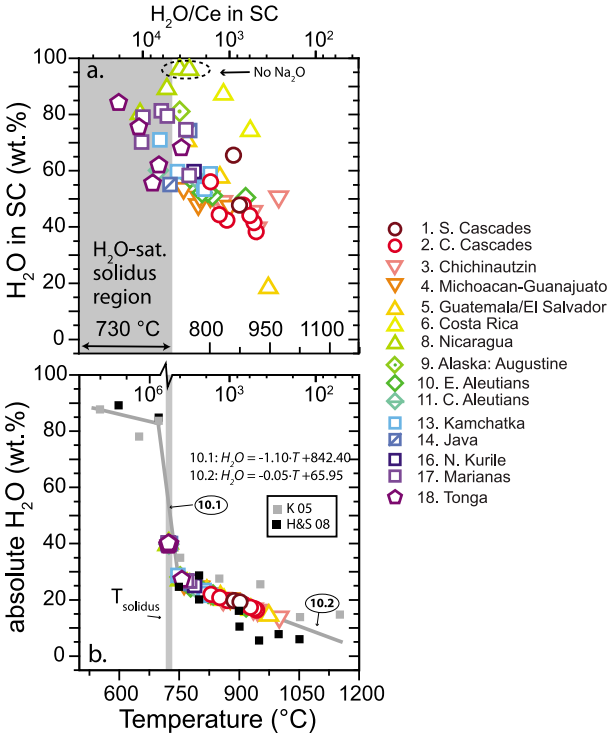

Figure 10. (a) Slab component H_2O contents (SC total normalized to 100 wt.%) calculated for each primitive magma plotted against temperature (calculated from SC H_2O/Ce using equation (2) in text; H_2O/Ce ratios shown along top axis). Symbols for SCs are as in Figures 1 and 9. Note that two SCs from Nicaragua (highlighted with a dashed oval) lack Na_2O (other compositions have ~15–20 wt.%) and so SC H_2O contents of these compositions are overestimated. (b) Absolute H_2O contents of slab components at 3.5–4.5 GPa determined by comparing H_2O contents from experimental run products of *Kessel et al.* [2005] (4 GPa; gray squares) and *Hermann and Spandler* [2008] (3.5–4.5 GPa; black squares) at equivalent temperatures. The temperatures for the Kessel et al. run products have been shifted down by 150°C after *Plank et al.* [2009] to account for the K-free bulk composition. The thick, gray line segments are linear regressions through the experimental data at 10.1: 725°C ≤ T ≤ 750°C, and 10.2: T ≥ 750°C (equations given at upper right).

Figure 9) could be reproduced with fractional dehydration/melting models using temperature-dependent fluid–solid bulk partition coefficients determined by experiment [*Kessel et al.*, 2005] for bulk sediment (GLOSS [*Plank and Langmuir*, 1998]) and altered oceanic crust ('Super'-AOC [*Kelley et al.*, 2003]) compositions. We used the fractional melting equation, rather than batch melting, to model the fluid composition released from the slab because we think that this should better approximate loss of components from the slab. Exponential functions were fit to the partitioning data for B, Ba, La, Ce, and Nb reported by *Kessel et al.* [2005] at 700–1000°C and 4 GPa (Table S2). By rearranging equation (2), we calculate the expected H_2O/Ce ratio in our models at each temperature and from these we calculated H_2O contents (using the concentration of Ce) in the modeled fluids. Cl contents in the modeled fluids were calculated assuming a constant H_2O/Cl ratio (Figure 5a). In general, our models are able to reproduce the positive trends observed in the magma and SC compositions (Figure 9), consistent with the interpretation that the observed correlations result from temperature variations in the SC. We point out that the elemental ratios of the modeled SCs are influenced predominantly by temperature and only slightly by source composition (GLOSS or AOC) and degree of dehydration/melting (F) (also note that the models in Figure 9 are isothermal and are connected along isopleths of F). As a result, these models are unable to distinguish between sediment-dominated versus AOC-dominated signals that have been observed in other studies [e.g., *Elliott et al.*, 1997; *Elliott*, 2003; *Eiler et al.*, 2005]. We recognize that these models are greatly simplified compared to the complex mixing and dehydration/melting processes occurring at depth, particularly because multiple fluid/melt sources likely contribute to the SCs beneath a particular arc segment. Additionally, the temperature-dependent bulk partition coefficients used in these models from *Kessel et al.* [2005] are appropriate for H_2O-saturated conditions of MORB-like bulk compositions and may not be applicable to other bulk compositions (i.e., GLOSS). Despite these caveats, we suggest that some of the variability in arc magmas previously attributed to either sediment-melt versus AOC-derived fluids (e.g., Marianas [*Elliott et al.*, 1997]) or differing sediment and/or mantle sources may ultimately result from variations in slab temperature.

[22] The calculated SCs represent the relative proportions of elements in the slab component contributing to each parent magma (Table 2). A broad decrease in the H_2O contents of the calculated SCs is observed in compositions inferred to have formed at elevated temperatures (lower H_2O/Ce ratios; Figure 10a). Insufficient knowledge regarding the behavior of major chemical components like MgO, FeO^T, Al_2O_3 and SiO_2 do not permit us to accurately calculate the absolute solute concentrations in the slab-derived components using the method described above [*Stolper and Newman*, 1994; *Portnyagin et al.*, 2007]. However, absolute H_2O

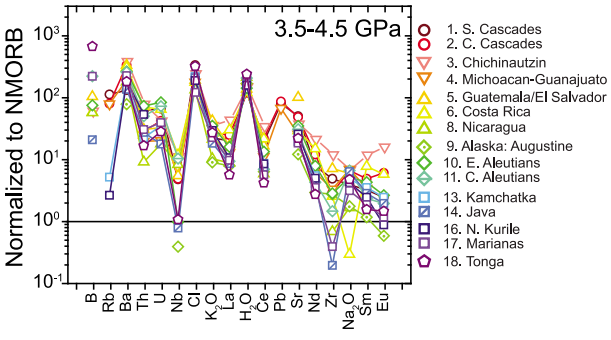

Figure 11. N-MORB normalized trace element plot of calculated average (±1 s.d.) subduction components at 3.5–4.5 GPa [*Sun and McDonough*, 1989; *McDonough and Sun*, 1995]. Symbols are as in Figures 1 and 9.

contents for the SCs at 3.5–4.5 GPa may be approximated by comparing SC temperatures calculated using equation (2) combined with the H_2O contents of the experimental run products (fluids and melts) from *Hermann and Spandler* [2008] and *Kessel et al.* [2005] at a given temperature (Figure 10b). Approximate absolute H_2O contents in the calculated SCs at 3.5–4.5 GPa are tabulated in Table 2 and shown in Figure 10b. Equation (10.1) in Figure 10b approximates the rapid change in H_2O concentration for fluids over the narrow temperature interval in the solidus region, but this is not well constrained experimentally. Thus, while the temperatures are not sensitive to large variations in H_2O/Ce in this region, the H_2O concentrations in SCs may not be completely accurate for high H_2O/Ce values (e.g., Tonga, Marianas). Therefore, we have chosen to fix the absolute H_2O contents of these SCs at the solidus temperature (730°C, ∼39–40 wt.% H_2O). Despite uncertainties, these approximations are useful to further emphasize the compositional distinctions apparent in SCs added to the mantle source beneath arcs characterized by cooler slabs and those characterized by warmer slabs. Approximate solute concentrations of the trace elements in the actual slab-derived fluids/melts at 3.5–4.5 GPa may be estimated by assuming a constant H_2O/element ratio in the SC and multiplying this ratio by the experimentally constrained H_2O contents (shown in Figure 10b).

[23] A MORB-normalized multielement plot of calculated SCs at 3.5–4.5 GPa emphasizes differences between arcs characterized by different thermal parameters (Figure 11). All of the slab components display LILE-enrichments over LREE along with negative Nb anomalies, but SCs in lower-Φ arc settings tend to be more solute-rich whereas those in higher-Φ arc settings appear to be more dilute (Figures 10 and 11). This observation is consistent with the expected transition of high-pressure slab-derived components from more dilute aqueous fluid-like compositions to hydrous slab melts with increasing temperature [*Kessel et al.*, 2005; *Hermann and Spandler*, 2008; *Plank et al.*, 2009]. Major differences in element concentrations are apparent for the LREEs, Rb, Nb and Zr: elements for which partitioning is predominantly controlled by the solubility of a single phase (i.e., monazite/allanite for LREEs, phengite for Rb, rutile for Nb, and zircon for Zr). In fact, the positive correlation observed between magmatic H_2O/Ce and Φ in Figure 8 is also observed for H_2O/Nb and H_2O/Zr. While not obvious from Figure 11, we also find that La/Sm ratios (commonly interpreted to reflect enrichment due to sediment addition [*Elliott*, 2003]) increase in arcs characterized by lower Φ. At typical sub-arc pressures (∼3.5–4.5 GPa), however, the slab is below the 2nd critical endpoint where aqueous fluids and hydrous melts would be miscible, so a single supercritical phase is not stable. Therefore, what we observe as an increase in concentration with slab temperature in the calculated SCs might actually result from a greater proportion of hydrous partial melts relative to AOC- or serpentinite-derived fluids (produced during dehydration) contributing to the overall SC in hotter (lower Φ) arc settings. Whatever the relative proportions of these different fluid components may be, the slab surface temperatures beneath arcs estimated from H_2O/Ce data suggest that the phase exiting the slab surface into the mantle wedge is a hydrous melt or solute-rich fluid, and so more dilute aqueous fluids released from the slab interior beneath the arc must ultimately induce flux melting at the slab top [*Cooper et al.*, 2012] while potentially imparting an aqueous fluid-like chemical and/or isotopic signature.

[24] Some studies have identified two distinct slab component contributions within a given arc segment, one being more dilute than the other [*Elliott et al.*, 1997; *Eiler et al.*, 2005; *Bezos et al.*, 2009; *Le Voyer et al.*, 2010]. Certain SC end-members may be distinguished from one another on the basis of oxygen isotopes because sediment melts are expected to be isotopically heavier than either AOC- or serpentinite-derived fluids [*Bindeman et al.*, 2005; *Eiler et al.*, 2005]. We examine the relationships between H_2O/Ce ratios of primitive arc magmas and $\delta^{18}O$ values of olivines crystallizing from these melts in Figure 12a and extend the Central American SC mixing model of *Eiler et al.* [2005] to encompass the global spectrum of arc

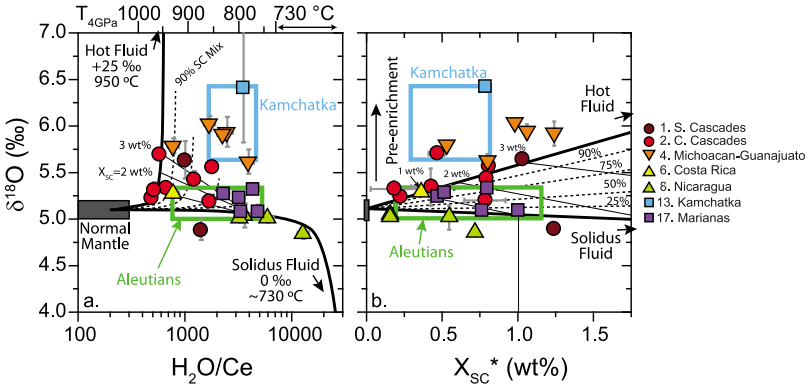

Figure 12. Oxygen isotope values for olivines ($\delta^{18}O_{olivine}$, ‰) plotted against (a) magmatic H_2O/Ce and (b) calculated amounts of equivalent slab component (X^*_{SC}, wt.%) added to the source mantle in melting models. Symbols are the same as those in Figure 1 with the addition of boxes encompassing the oxygen isotope and H_2O/Ce ranges for magmas from the Aleutians and Kamchatka. Ranges for oxygen isotopes in the mantle and magmas from the Aleutians and Kamchatka are from *Bindeman et al.* [2005]. Ranges in H_2O/Ce and X^*_{SC} are from the vents in this study (i.e., the vents used to determine H_2O/Ce were not the same vents sampled for oxygen isotope analyses). Error bars for $\delta^{18}O_{olivine}$ are 1 standard deviation from the mean, those shown for H_2O/Ce are approximated to be ~12% relative and are smaller than the symbols. Temperatures along the top axis of Figure 12a correspond to those calculated from the H_2O/Ce slab fluid geothermometer of *Plank et al.* [2009] at 3.5–4.5 GPa (equation (2) in text). Error bars for X^*_{SC} for Central and Southern Cascades were estimated using Monte Carlo methods (see text). Thick black lines represent mixing lines between a mantle source (H_2O/Ce = 200, $\delta^{18}O_{olivine}$ = 5.1‰) and two end-member slab components: a 'Hot Fluid' at 950°C (H_2O/Ce = 637) with 17 wt.% H_2O [after *Plank et al.*, 2009] and $\delta^{18}O_{olivine}$ = +25‰ [after *Eiler et al.*, 2005] and a cooler 'Solidus Fluid' representing a serpentinite-derived fluid ($\delta^{18}O_{olivine}$ = 0‰) at the H_2O-saturated sediment solidus (730°C, H_2O/Ce = 30,000) containing 50 wt.% H_2O. Thin dashed lines represent mixing paths between the mantle and bulk mixtures of the two end-member slab fluid components (proportions labeled in Figure 12b). Thin solid lines contour amounts of actual slab component addition (X_{SC} in wt.%) to the mantle source. Arrow in Figure 12b indicates direction of pre-enrichment of the mantle wedge by previous subduction activity [*Bindeman et al.*, 2005]. The abscissa in Figure 12b is shown as equivalent slab component rather than actual amount of slab melt component added (thin solid lines). This is necessary because the lower H_2O contents in the hotter slab fluids compared to the cool 'Solidus Fluid' require more mass addition to produce magmas with equivalent H_2O contents. The relationship between X^*_{SC} and actual X_{SC} is approximated by the mass balance equation: $X^*_{SC} = X_{SC} \cdot (C^{H_2O}_{hotfluid} - C^{H_2O}_{mantle})/(C^{H_2O}_{solidus} - C^{H_2O}_{mantle})$, where X_{SC} and $C^{H_2O}_{hotfluid}$ are the actual amounts of 'Subduction Component' added and H_2O contents of a slab fluid, respectively. The terms $C^{H_2O}_{solidus}$ and $C^{H_2O}_{mantle}$ are the H_2O contents in the 'Solidus Fluid' (T ~730°C) and mantle source, respectively.

magmas. While a clear mixing relationship is not apparent, the majority of our data can be reproduced by mixing models between a mantle source ($\delta^{18}O_{olivine}$ = 5.1‰, H_2O/Ce = 200) and a variable subduction component that is itself a mixture between two end-member hydrous melts: a hot (950°C, H_2O/Ce = 637) hydrous (17 wt.% H_2O) sediment melt with $\delta^{18}O_{olivine}$ = +25‰ and a cooler (~730°C with H_2O/Ce ~ 10^4 [*Plank et al.*, 2009; *Cooper et al.*, 2012]) melt at the H_2O-saturated sediment solidus (~50 wt.% H_2O) isotopically similar to a serpentinite-derived fluid ($\delta^{18}O_{olivine}$ = 0‰). End-member H_2O contents and temperatures used here are after *Plank et al.* [2009, and references therein] along with oxygen isotopic values from *Eiler et al.* [2005] – note that we have used a low $\delta^{18}O_{olivine}$ value corresponding to serpentinite-derived fluids, less extreme $\delta^{18}O_{olivine}$ values (i.e., >0‰) could also be used without significantly affecting the model results. Figure 12b shows that the mixing models agree reasonably well with the calculated amounts of SC required by the mantle-melting calculations, lending additional credibility to these models (Section 4.2.1). Some magmas from Mexico (MGVF) and Kamchatka contain olivines with elevated $\delta^{18}O$ values that cannot be adequately explained by these mixing models alone. These magmas, however, have been interpreted to reflect formation in an isotopically heavy mantle wedge that had been pre-enriched by slab-derived fluids beneath the forearc prior to slab roll-back (MGVF [*Johnson et al.*, 2009]; S. Cascades [*Martin et al.*, 2011]) or terrane docking accompanied by trench-ward arc migration (Kamchatka [*Auer et al.*, 2009]).

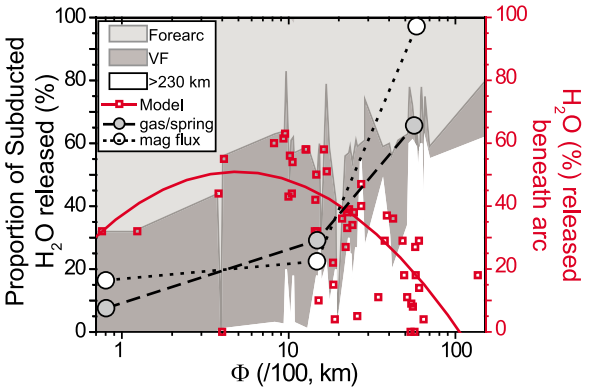

Figure 13. Proportions of mineralogically bound slab H_2O released beneath the forearc (light gray; depth < VF), the arc (dark gray; VF ≤ depth < 230 km) and the deeper mantle (white; depth ≥ 230 km) as predicted for a global compilation of arcs by geodynamic models [*van Keken et al.*, 2011]. Red open squares correspond to the right-hand axis and show the proportion of H_2O released beneath the volcanic arc (dark gray shaded field). These values have been fit with a quadratic expression to emphasize the predicted maximum sub-VF dehydration efficiency beneath arcs characterized by intermediate Φ values. Estimated magmatic H_2O recycling efficiencies calculated from melt inclusion (magmatic flux: white) and degassing plume/spring water data (gray) for the Central Cascades, CAVA, and Kamchatka-Kurile from Table 3 (using serpentinized mantle inputs) are shown for comparison.

4.3. Magmatic Volatile Fluxes and Recycling Efficiencies

[25] Geodynamic models combined with thermodynamic constraints predict that shallow slab dehydration in hot (low-Φ) arc settings should lead to a decrease in the amount of H_2O being fluxed into the mantle wedge at sub-arc depths compared to cooler (high-Φ) settings [*Peacock*, 2003; *van Keken et al.*, 2011]. Significant shallow dehydration would also inhibit the transport of volatiles into the deeper mantle. The converse should be true for arc segments characterized by extremely high Φ values (e.g., Tonga) as dehydration beneath the forearc is predicted to be negligible and hydrous phase stability is increased at greater depths (Figure 2) [*Hacker*, 2008; *van Keken et al.*, 2011]. Arcs with the hottest slabs (e.g., Cascades) are predicted to lose ∼68% of structurally bound H_2O prior to reaching depths below the VF while the remaining ∼32% is lost beneath the arc [*van Keken et al.*, 2011]. Cooler slabs (e.g., Kamchatka) are predicted to lose 30–40% of structurally bound H_2O beneath the forearc and transport ∼40% into the deep mantle, leaving only ∼20% of the incoming H_2O available to flux the mantle wedge beneath the VF. The trade-off between forearc dehydration and high pressure hydrous phase stability should manifest in an optimum arc setting where slab-derived volatiles are most efficiently returned to the sub-arc mantle. A summary of the geodynamic models of *van Keken et al.* [2011] suggests that optimum slab recycling occurs beneath arcs characterized by intermediate Φ values of ∼800–1200 km (Figures 4a and 13). Intriguingly, the highest primitive melt H_2O, Cl and S contents also occur in arcs with intermediate Φ values (Figure 5), but it is not clear if these are statistically meaningful given the extensive overlap of volatile contents between intermediate- and high-Φ arcs.

[26] Magmatic volatile fluxes estimated from volcanic outputs may be expected to reflect slab fluxes beneath volcanic arcs. In this section, we examine volatile fluxes for three well studied arcs representing a range in slab conditions: the Central Cascades (Φ = 80 km), Central America (Φ = 1000–1100 km), and Kamchatka-Kurile arcs (Φ = 5400–6400 km). We then compare these estimates to the slab dehydration estimates from *van Keken et al.* [2011]. Previous studies have used data from passively degassing volcanoes and geothermal systems to estimate volatile fluxes in the Central American Volcanic Arc (CAVA [*Hilton et al.*, 2002; *Sadofsky et al.*, 2008]) and the Kamchatka-Kurile arc (KK [*Taran*, 2009]) (Table 3). Here we estimate the major volatile fluxes for the Central Cascades, but we note that estimates and comparisons with other arcs are not straightforward because there are no passively degassing volcanoes in the area. Therefore, we have constrained magmatic volatile fluxes (H_2O, S, Cl, and CO_2) from the Central Cascades using two approaches.

[27] We first constrained volatile fluxes for the Cascades by combining the average volatile contents for Central Cascades primitive magmas (Table 1) with estimated magma supply rates constrained from geochronological studies. Using a constant extrusive production rate of ∼5 km^3/km of arc/Ma over the past 2 Ma [*Sherrod and Smith*, 1990] and assuming an intrusive: extrusive ratio of ∼5:1 [*White et al.*, 2006] yields a magma production rate of ∼30 km^3/km of arc/Ma for the Central Cascades. This is comparable to the magmatic production rates (9–33 km^3/km of arc/Ma) inferred by *Ingebritsen et al.* [1989] using regional heat flow data. Assuming an average magma density of 2.8 g/cm^3, we obtain a magma flux estimate of 8.40×10^7 kg/km/yr. Combining this estimate with the average parental melt volatile contents yields

Table 3. Magmatic Volatile Fluxes and Recycling Efficiencies

	Central Cascades (Avg Φ = 80 km)	Central America (Avg Φ = 1150) *Sadofsky et al.* [2008]	Kamchatka-Kurile (Avg Φ = 5900) *Taran* [2009]	Global Arc Averages
Volcanic Flux[a] (kg/km/yr)	1.40E+07	2.80E+07	1.62E+08	-
Magma Flux[b] (kg/km/yr)	8.40E+07	1.68E+08	9.74E+08	1.41E+08
		Parent Melt Composition[c] *(wt%)*		
H_2O	2.3 ± 0.6	3.6 ± 1.4	3.0 ± 0.7	3.3 ± 1.2
Cl	0.05 ± 0.02	0.08 ± 0.03	0.08 ± 0.20	0.09 ± 0.05
S	0.10 ± 0.03	0.21 ± 0.9	0.17 ± 0.08	0.16 ± 0.09
CO_2[d]	1.0 ± 0.3	1.0 ± 0.3	1.0 ± 0.3	1.0 ± 0.3
		Fluxes (kg/km/yr × 10^4)		
	Magma/Springs	Magma/Plumes	Magma/Springs	Magma
H_2O flux	193/78	605/836[e]	2920/1980[f]	470
Cl flux	4.2/1.7	13.4/18.0[e]	78.0/19.0[f]	12.7
S flux	8.4/3.4	35.3/64.5[e]	166.0/71.0[f]	22.5
CO_2 flux	84/34[g]	168/175[h]	974/97[f]	141
		Slab Inputs (kg/km/yr × 10^4)		
H_2O[i]	1120 (770)	2770 (1590)	3020 (1500)	2590 (1790)
Cl	13.7[j]	100.0[e]	57.0[f]	13.7[j]
S	297[h]	297[h]	170[f]	297[h]
CO_2	251[h]	1225[k]	480[f]	340[d]
		Recycling Efficiencies[l] *(%)*		
	Magma/Springs	Magma/Gas	Magma/Springs	Magma
H_2O[i]	17(25)/8(12)	22(38)|30(53)	97(*195*)|66(*132*)	18 (26)
Cl	31/12	13/18	*137*/33	93
S	3/1	12/22	97/42	8
CO_2	33/14	14/14	*203*/20	41
H_2O lost to forearc[m] (%)	68	∼30 (18–37)	28	∼40
H_2O lost to mantle[n] (%)	0	∼13 (2–20)	61	∼27

[a]Central Cascades: average mafic extrusive flux from *Sherrod and Smith* [1990] for the past 2 Ma; Central America: *Sadofsky et al.* [2008]; Kamchatka-Kurile: average mafic extrusive flux for the Central Kamchatka Depression and the Eastern volcanic front over the Holocene from *Ponomareva et al.* [2007].

[b]Assuming an average intrusive-extrusive ratio of 5:1 [*White et al.*, 2006]. Global average using 2.5 km^3/yr from *Carmichael* [2002] and global arc length of 44,454 km [*Jarrard*, 2003].

[c]Average volatile contents (±1 s.d.) of Central Cascades, Central America, and Kamchatka magmas from this study.

[d]After *Wallace* [2005].

[e]From *Sadofsky et al.* [2008].

[f]From *Taran* [2009].

[g]From *James et al.* [1999].

[h]From *Hilton et al.* [2002].

[i]Using H_2O inputs from *van Keken et al.* [2011] models with serpentine and without (values in parentheses) serpentine in the subducting lithospheric mantle.

[j]Global average Cl in subducting plates from *Ito et al.* [1983].

[k]From *Jarrard* [2003].

[l]Volatile recycling efficiencies calculated using volatile fluxes for volcanic, magmatic, and spring/gas estimates and slab input estimates. Values over 100% are italicized.

[m]% H_2O lost from the slab at depths < VF (depth to CAVA VF determined from *Carr et al.* [2003]; dehydration models of *van Keken et al.* [2011]).

[n]% H_2O remaining in slab at depths > 230 km [*van Keken et al.*, 2011].

maximum fluxes (in kg/km/yr) of 1.93×10^6 H_2O, 4.2×10^4 Cl, and 8.4×10^4 S. Carbon dioxide contents in melt inclusions are generally poor constraints on initial magmatic CO_2 values because of (1) significant degassing prior to melt inclusion entrapment and (2) continued degassing into post-entrapment shrinkage bubbles prior to quenching [*Anderson and Brown*, 1993; *Wallace*, 2005; *Metrich and Wallace*, 2008; *Blundy et al.*, 2010]. Therefore, using an estimate of ∼1.0 wt.% initial CO_2 in the arc magmas [*Wallace*, 2005], we calculate a CO_2 flux of 8.4×10^5 kg/km/yr for the Central Cascades. The calculated CO_2 and Cl fluxes are slightly higher than, but still comparable to, the values of 3.4×10^5 and 1.5×10^4 kg/km/yr for CO_2 and Cl, respectively, obtained from Central

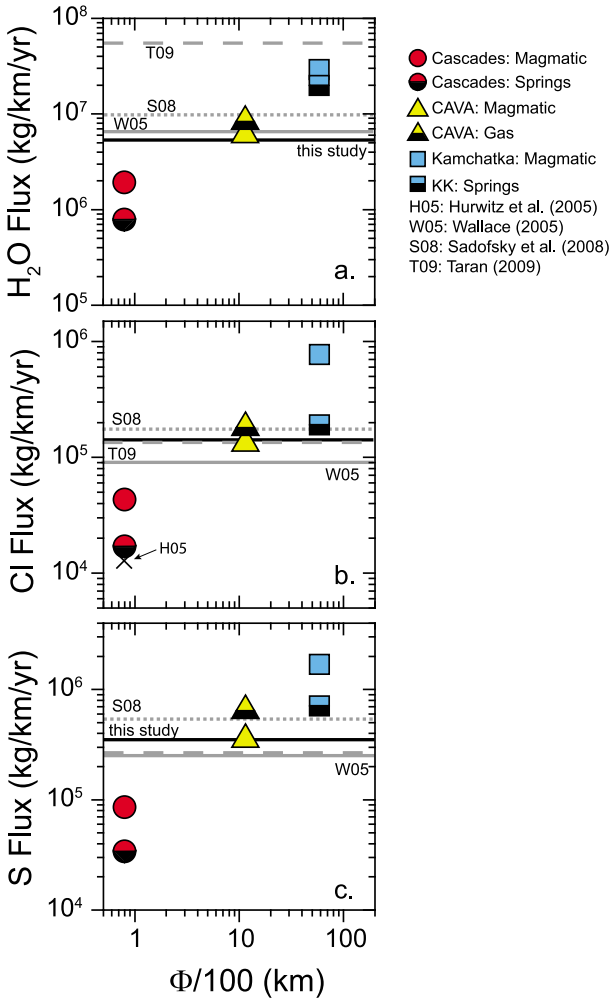

Figure 14. Volatile flux estimates for (a) H_2O, (b) Cl, and (c) S in kg/km arc/yr as calculated in the text and reported in Table 3. Symbols are shown in the legend with half-filled symbols representing flux estimates using spring water and/or degassing measurements. Average global flux estimates are also shown from *Wallace* [2005] (solid gray line), *Sadofsky et al.* [2008] (dotted gray line), *Taran* [2009] (dashed gray line), and this study (solid black line). These were calculated using a global arc length of 44,454 km [*Jarrard*, 2003]. The magmatic Cl flux estimate for the Central Cascades determined by spring waters in the study of *Hurwitz et al.* [2005] is also shown for comparison in Figure 14b.

Cascades spring waters [*James et al.*, 1999; *Hurwitz et al.*, 2005] (Table 3).

[28] We also estimate Central Cascades fluxes using a second approach that is based on an initial primitive magma CO_2 content of ~1 wt.%, which, as shown above, is consistent with the spring water data. Primitive magma ratios of H_2O, S, and Cl to CO_2 are multiplied by the CO_2 flux estimate of *James et al.* [1999] to yield volatile flux estimates (in kg/km/yr) of 7.82×10^5 H_2O, 1.7×10^4 Cl, and 3.4×10^4 S. This second method yields fluxes that are ~40% lower than those estimated above using magmatic fluxes, but again yields results comparable to the Cl flux estimate of *Hurwitz et al.* [2005] (Figure 14b and Table 3). Relatively good agreement between these two methods also suggests that our calculations are reasonably well constrained and that the low fluxes are not simply due to the Cascades magmatic flux estimates being at the low end of predicted magma supply rates for other arcs [cf., *Crisp*, 1984; *Sadofsky et al.*, 2008]. In these calculations, we have used primitive melt volatile contents for subduction-related magmas in the Central Cascades in both approaches. Therefore, all of the volatile fluxes reported are maxima because the relative proportions of primitive extension-related magmas (which have lower volatile contents) and subduction-related magmas entering the Central Cascades crust are not currently known.

[29] To ensure that our magmatic flux comparisons are robust, we have also calculated the volatile flux estimates for the Central American and Kamchatka arcs using total magmatic fluxes (assuming a 5:1 intrusive-extrusive ratio [*White et al.*, 2006]) of 1.68×10^8 [after *Sadofsky et al.*, 2008] and 9.74×10^8 [after *Ponomareva et al.*, 2007], respectively, along with the average parental melt volatile contents determined in this study (Table 1). Volatile flux estimates are tabulated in Table 3 and plotted against slab thermal parameter in Figure 14. Fluxes estimated for CAVA using the magma flux approach (here) and those estimated from plume data [*Sadofsky et al.*, 2008] are in good (to within a factor of 2) agreement (Table 3). For Kamchatka, flux estimates calculated using a constant magma flux are 1.5 to 10 times larger than those estimated using spring waters (Table 3) [*Taran*, 2009]. For completeness, we also calculated global average arc volatile flux estimates using the data compiled here (Table 1) and an average magma flux rate of 1.41×10^8 kg/km/yr [after *Carmichael*, 2002; *Wallace*, 2005]. Our calculations yield average global arc volatile fluxes (in kg/km/yr) of 4.70×10^6 H_2O, 1.30×10^5 Cl, 2.30×10^5 S, and 1.40×10^6 CO_2 (Table 3), comparable to within an order of magnitude to previous estimates reported by *Wallace* [2005] normalized per km of arc length.

[30] Figure 14 compares the magmatic volatile fluxes (H_2O, Cl, and S) estimated here with those estimated for the CAVA (Table 3) [*Sadofsky et al.*, 2008] and the KK systems (Table 3) [*Taran*, 2009] along with average global volatile flux estimates normalized per km of arc length. Flux estimates for

Central Oregon are up to an order of magnitude below the estimated global averages and the estimates for the CAVA and KK systems. Flux estimates for the KK system are generally higher than or equal to global average flux estimates per km of arc length. A potential positive trend is suggested in Figure 14 between magmatic volatile flux and slab thermal parameter, however, uncertainties in individual flux estimates are large (potentially up to 100% [cf., *Taran*, 2009]). Despite large uncertainties, consistency between flux estimates calculated using differing approaches lends credibility to these observations. A positive trend between volatile fluxes and Φ, however, might not be expected because while most of the slab-derived volatiles should be released beneath the forearc in a hot slab setting (low-Φ), significant amounts of volatiles should also be transported into the deeper mantle by cooler slabs (higher-Φ).

[31] Maximum volatile recycling efficiencies (defined here as magmatic output flux divided by the structurally bound slab input flux) for the Central Cascades, CAVA, and KK systems were estimated from the volatile flux rates determined above and the incoming volatile fluxes estimated for subducting slabs (sources in Table 3). Magmatic H_2O and S recycling efficiencies are lower in the Central Cascades than those estimated for the Central American and Kamchatka-Kurile arcs. Chlorine and CO_2 recycling efficiencies are similar between the Central Cascades and CAVA. In general, the recycling efficiencies calculated using flux rates determined by magmatic inputs and those calculated using spring/gas discharges are comparable for both the CAVA and the Central Cascades. Recycling efficiency estimates reported for the Kamchatka-Kurile system, however, show greater discrepancies between the magma-determined and spring-determined flux calculations (Table 3). Both methods, however, suggest that recycling efficiencies for all volatiles are higher in the KK system than in either the Central Cascades or CAVA. Global average arc recycling efficiencies for Cl and S calculated here are generally in agreement with estimates made by *Wallace* [2005] where subducted input and arc output Cl fluxes are roughly balanced and only a small amount of subducted S is returned to the surface via arc magmatism. There is an apparent discrepancy, however, between previous studies suggesting that global magmatic recycling efficiencies for H_2O are close to 100% [*Hilton et al.*, 2002; *Wallace*, 2005] and our results predicting that only about 18–26% of structurally bound H_2O is recycled back to the surface via arc volcanism (Table 3). Previous H_2O recycling efficiency estimates are also at odds with recent geodynamic models predicting that a global average of ∼30% of incoming H_2O is recycled to the deep mantle [*van Keken et al.*, 2011], whereas the former estimates would suggest that little slab-derived H_2O is returned to the deep mantle or stored within a serpentinized forearc. This discrepancy mostly results from the considerably different estimates of incoming subducting H_2O fluxes between *Hilton et al.* [2002] (∼5×10^6 kg/km/yr) and *van Keken et al.* [2011] (∼1.8×10^7 and ∼2.6×10^7 kg/km/yr for models excluding and including serpentinite in the subducting lithospheric mantle, respectively). Our results also suggest that Cl is more efficiently recycled back to the surface via arc magmatism than H_2O, implying a fractionation that is not apparent in the relatively constant global arc H_2O/Cl magma values (Figure 6). Alternatively, the estimated global average arc recycling efficiency for Cl significantly decreases down to ∼23% if the global input flux (∼2.5×10^{13} g/yr) of *Jarrard* [2003] is used, however this estimate was made using pore H_2O trapped within the subducting slab that would largely be squeezed out prior to dehydration at shallow depths.

[32] For the purposes of comparing estimated H_2O recycling efficiencies for the arcs studied here with geodynamic models, we normalize the calculated H_2O fluxes in Table 3 to the structurally bound H_2O inputs used in the work of *van Keken et al.* [2011]. Figure 13 shows a comparison between the three arcs examined here and the geodynamic models (compare dashed and dotted lines to red curve). Estimated H_2O recycling efficiencies are lower than the predicted amounts of H_2O released into the mantle wedge beneath the Central Cascades and Central American volcanic fronts by about a factor of two, whereas calculated H_2O recycling efficiencies for the Kamchatka-Kurile system are considerably higher than those predicted by the geodynamic models. These observations imply that either (1) much of the slab-derived H_2O beneath released beneath the Central Cascades and CAVA never reaches the surface whereas an additional H_2O source may exist at depth beneath the Kamchatka-Kurile arc – perhaps related to the old, serpentinized forearc that contributes heavy oxygen isotope values to the erupted magmas (Figure 12); or (2) magmatic volatile recycling efficiencies are largely influenced by the absolute H_2O-contents of the slab-derived fluids. This latter interpretation is

supported by calculated SCs and experimental run products which both indicate that cooler slab-derived fluids are considerably more H_2O-rich than their warmer counterparts (Figure 10 and Table 2). This interpretation also suggests that magmatic volatile recycling efficiencies are decoupled from sub-arc slab-fluid fluxes, the former reflecting the composition of the slab-derived fluid and the latter reflecting the slab thermal structure.

5. Conclusions

[33] We have compiled a data set of primitive magma compositions for 100 volcanic centers comprising 18 arc segments encompassing the global range in slab thermal parameter. We demonstrated that magmatic volatile (H_2O, S, Cl) and B contents are more variable and extend to greater values in magmas erupted from edifices located at distances of ~90–120 km above the subducting slab compared to those erupted farther from the trench, where depth to the slab is greater. These observations are consistent with major dehydration reactions predicted to occur at similar depths by recent geodynamic models (Figure 4) and provide clear evidence that magmatic volatiles are ultimately derived from the dehydrating subducting slab. Weak positive correlations exist between H_2O and Cl, B, and S for the global data set, but H_2O contents are not necessarily correlated with many LILEs, such as Ba (Figure 6). Significant positive correlations between H_2O/Ce and slab tracers such as Ba/La, B/La, and Cl/Nb suggest that magmas generated in hotter (low-Φ) arc settings have more muted subduction-related signals than those generated in cooler (higher Φ) settings (Figure 7). Magmatic H_2O/Ce ratios are positively correlated with Φ and do not correlate with Ce contents of incoming sediment packages. Instead, higher H_2O/Ce ratios reflect lower sub-arc slab surface temperatures for older, faster subducting plates (Figure 8).

[34] We infer that H_2O/Ce, Cl/Nb, B/La, and Ba/La ratios characteristic of the subduction component are largely preserved in the parent magma compositions studied here. The positive correlations between volatile/trace element ratios of the global data set are reproduced by fractional dehydration/melting models of generic subducting materials over the range of temperatures inferred for slab surfaces at sub-arc depths (Figure 9). Further, bulk mixing models between the mantle wedge and a spectrum of SCs (defined by mixtures between end-member H_2O-rich (~50 wt.%) sediment melts at the wet sediment solidus isotopically similar to serpentinite-derived fluids and hotter H_2O-poor (~17 wt.%), isotopically heavier sediment melts are able to reproduce the oxygen isotope compositions of olivine phenocrysts that crystallize from arc basalts (Figure 12). We suggest that observed correlations involving volatile and trace element ratios do not result from mixing between a MORB source and a single volatile-rich fluid component. Rather, the data reflect genuine changes in the nature of the slab-derived component, which has higher trace element to H_2O ratios in arcs with hotter slabs due to the effect of temperature on element partitioning (Figures 9–12).

[35] We also calculated maximum magmatic volatile flux estimates (H_2O, S, and Cl) for the Central Cascades using two different methods. Magmatic volatile flux estimates for the Cascades are up to one order of magnitude less than those estimated for the fluxes from the Central American and Kamchatka-Kurile systems (Figure 14). The majority of slab-derived H_2O becomes trapped within a serpentinized forearc above slabs characterized by low-Φ values, consistent with geophysical evidence, whereas cooler slabs (high-Φ) recycle significant amounts of H_2O into the deep (>230 km) mantle. Geodynamic models predict that an optimum 'sweet-spot' exists for slabs with Φ-values ~ 900–1200 km, where maximum fluid release should occur beneath the VF, however this prediction is not supported by current flux estimates. Lack of agreement between the flux and recycling efficiency estimates with those from geodynamic models may indicate decoupling between slab fluid release and absolute volatile addition to the mantle wedge arising from temperature-dependent compositional changes of the slab-derived component. However, considerable uncertainties associated with magmatic volatile flux estimates calculated from melt inclusions and/or fumarole gases along with potentially high arc to arc variability of H_2O bound in subducting serpentinites may obscure modeled correlations and highlight the need for more volatile flux constraints from additional arcs.

Acknowledgments

[36] We thank Peter van Keken and Ellen Syracuse for providing geodynamic modeling results. We also thank Nathalie Vigouroux for providing unpublished melt inclusion data for Kawah Ijen volcano. Additionally, the constructive reviews and suggestions by Jim Walker and Maxim Portnyagin were greatly appreciated. This work was funded by the National Science Foundation (EAR-0440394 to PJW) and a 2008 USGS Kleinman award and 2008 GSA grant to DMR.

References

Anderson, A. T., and G. G. Brown (1993), CO_2 contents and formation pressures of some Kilauean melt inclusions, *Am. Mineral.*, *78*(7–8), 794–803.

Auer, S., I. Bindeman, P. Wallace, V. Ponomareva, and M. Portnyagin (2009), The origin of hydrous, high-$\delta^{18}O$ voluminous volcanism: Diverse oxygen isotope values and high magmatic water contents within the volcanic record of Klyuchevskoy volcano, Kamchatka, Russia, *Contrib. Mineral. Petrol.*, *157*, 209–230, doi:10.1007/s00410-008-0330-0.

Benjamin, E. R., T. Plank, J. A. Wade, K. A. Kelley, E. H. Hauri, and G. E. Alvarado (2007), High water contents in basaltic magmas from Irazu Volcano, Costa Rice, *J. Volcanol. Geotherm. Res.*, *168*, 68–92, doi:10.1016/j.jvolgeores.2007.08.008.

Bezos, A., S. Escrig, C. H. Langmuir, P. J. Michael, and P. D. Asimow (2009), Origins of chemical diversity of back-arc basin basalts: A segment-scale study of the Eastern Lau Spreading Center, *J. Geophys. Res.*, *114*, B06212, doi:10.1029/2008JB005924.

Bindeman, I. N., J. M. Eiler, G. M. Yogodzinski, Y. Tatsumi, C. R. Stern, T. L. Grove, M. Portnyagin, K. Hoernle, and L. V. Danyushevsky (2005), Oxygen isotope evidence for slab melting in modern and ancient subduction zones, *Earth Planet. Sci. Lett.*, *235*(3–4), 480–496, doi:10.1016/j.epsl.2005.04.014.

Blundy, J., K. V. Cashman, A. Rust, and F. Witham (2010), A case for CO_2-rich arc magmas, *Earth Planet. Sci. Lett.*, *290*(3–4), 289–301, doi:10.1016/j.epsl.2009.12.013.

Bolge, L. L., M. J. Carr, K. I. Milidakis, F. N. Lindsay, and M. D. Feigenson (2009), Correlating geochemistry, tectonics, and volcanic volume along the Central American volcanic front, *Geochem. Geophys. Geosyst.*, *10*, Q12S18, doi:10.1029/2009GC002704.

Borg, L. E., J. Blichert-Toft, and M. A. Clynne (2002), Ancient and modern subduction zone contributions to the mantle sources of lavas from the Lassen Region of California inferred from Lu-Hf isotopic systematics, *J. Petrol.*, *43*(4), 705–723, doi:10.1093/petrology/43.4.705.

Bouvier, A.-S., N. Metrich, and E. Deloule (2008), Slab-derived fluids in magma sources of St. Vincent (Lesser Antilles Arc): Volatile and light element imprints, *J. Petrol.*, *49*, 1427–1448, doi:10.1093/petrology/egn031.

Bouvier, A.-S., E. Deloule, and N. Metrich (2010), Fluid inputs to magma sources of St. Vincent and Grenada (Lesser Antilles): New insights from trace elements in olivine-hosted melt inclusions, *J. Petrol.*, *51*(8), 1597–1615, doi:10.1093/petrology/egq031.

Carmichael, I. S. E. (2002), The andesite aqueduct: Perspectives on the evolution of intermediate magmatism in west-central (105–99°W) Mexico, *Contrib. Mineral. Petrol.*, *143*, 641–663, doi:10.1007/s00410-002-0370-9.

Carr, M. J., M. D. Feigenson, L. C. Patino, and J. A. Walker (2003), Volcanism and geochemistry in Central America: Progress and problems, in *Inside the Subduction Factory*, *Geophys. Monogr. Ser.*, vol. 138, edited by J. Eiler, pp. 153–174, AGU, Washington, D. C., doi:10.1029/138GM09.

Cervantes, P., and P. J. Wallace (2003), Role of H_2O in subduction-zone magmatism: New insights from melt inclusions in high-Mg basalts from central Mexico, *Geology*, *31*(3), 235–238, doi:10.1130/0091-7613(2003)031<0235:ROHOIS>2.0.CO;2.

Cooper, L. B. (2010), Volatiles in Tonga Arc magmas and their role in unraveling subduction zone processes, Ph.D. thesis, Boston Univ., Boston, Mass.

Cooper, L., T. Plank, R. J. Arculus, E. H. Hauri, P. S. Hall, and S. W. Parman (2010), High-Ca boninites from the active Tonga Arc, *J. Geophys. Res.*, *115*, B10206, doi:10.1029/2009JB006367.

Cooper, L. B., D. M. Ruscitto, T. Plank, P. J. Wallace, E. M. Syracuse, and C. E. Manning (2012), Global variations in H_2O/Ce: 1. Slab surface temperatures beneath volcanic arcs, *Geochem. Geophys. Geosyst.*, *13*, Q03024, doi:10.1029/2011GC003902.

Crawford, W. C., J. A. Hildebrand, L. M. Dorman, S. C. Webb, and D. A. Wiens (2003), Tonga Ridge and Lau Basin crustal structure from seismic refraction data, *J. Geophys. Res.*, *108*(B4), 2195, doi:10.1029/2001JB001435.

Crisp, J. A. (1984), Rates of magma emplacement and volcanic output, *J. Volcanol. Geotherm. Res.*, *20*, 177–211, doi:10.1016/0377-0273(84)90039-8.

Dixon, J. E., L. Leist, C. Langmuir, and J. G. Schilling (2002), Recycled dehydrated lithosphere observed in plume-influenced mid-ocean-ridge basalt, *Nature*, *420*, 385–389, doi:10.1038/nature01215.

Dreyer, B. M., J. D. Morris, and J. B. Gill (2010), Incorporation of subducted slab-derived sediment and fluid in arc magmas: B-Be-^{10}Be-εNd systematics of the Kurile convergent margin, Russia, *J. Petrol.*, *51*(8), 1761–1782, doi:10.1093/petrology/egq038.

Eiler, J. M., A. Crawford, T. Elliott, K. A. Farley, J. W. Valley, and E. M. Stolper (2000), Oxygen isotope geochemistry of oceanic arc lavas, *J. Petrol.*, *41*, 229–256, doi:10.1093/petrology/41.2.229.

Eiler, J. M., M. J. Carr, M. Reagan, and E. Stolper (2005), Oxygen isotope constraints on the sources of Central American arc lavas, *Geochem. Geophys. Geosyst.*, *6*, Q07007, doi:10.1029/2004GC000804.

Elliott, T. (2003), Tracers of the slab, in *Inside the Subduction Factory*, *Geophys. Monogr. Ser.*, vol. 138, edited by J. Eiler, pp. 23–45, AGU, Washington, D. C., doi:10.1029/138GM03.

Elliott, T., T. Plank, A. Zindler, W. White, and B. Bourdon (1997), Element transport from slab to volcanic front at the Mariana arc, *J. Geophys. Res.*, *102*(B7), 14,991–15,019, doi:10.1029/97JB00788.

George, R. M. M., S. P. Turner, C. J. Hawkesworth, J. D. Morris, C. J. Nye, J. G. Ryan, and S.-H. Zheng (2003), Melting processes and fluid and sediment transport rates along the Alaska-Aleutian arc from an integrated U-Th-Ra-Ba isotope study, *J. Geophys. Res.*, *108*(B5), 2252, doi:10.1029/2002JB001916.

Gill, J. B. (1981), *Orogenic Andesites and Plate Tectonics*, Springer, Berlin.

Gorbatov, A., and V. Kostoglodov (1997), Maximum depth of seismicity and thermal parameter of the subducted slab: A general empirical relation and its application, *Tectonophysics*, *277*, 165–187, doi:10.1016/S0040-1951(97)00084-X.

Gribble, R. F., R. J. Stern, S. H. Bloomer, D. Stuben, T. O'Hearn, and S. Newman (1996), MORB mantle and subduction components interact to generate basalts in the southern Mariana Trough back-arc basin, *Geochim. Cosmochim. Acta*, *60*(12), 2153–2166, doi:10.1016/0016-7037(96)00078-6.

Grove, T. L., S. Parman, S. Bowring, R. Price, and M. Baker (2002), The role of an H_2O-rich fluid component in the

generation of primitive basaltic andesites and andesites from the Mt. Shasta region, N California, *Contrib. Mineral. Petrol.*, *142*, 375–396, doi:10.1007/s004100100299.

Grove, T. L., C. B. Till, E. Lev, N. Chatterjee, and E. Medard (2009), Kinematic variables and water transport control the formation and location of arc volcanoes, *Nature*, *459*, 694–697, doi:10.1038/nature08044.

Gurenko, A. A., A. B. Belousov, R. B. Trumbull, and A. B. Sobolev (2005), Explosive basaltic volcanism of the Chikurachki volcano (Kurile arc, Russia): Insights on pre-eruptive magmatic conditions and volatile budget revealed from phenocryst-hosted melt inclusions and groundmass glasses, *J. Volcanol. Geotherm. Res.*, *147*, 203–232, doi:10.1016/j.jvolgeores.2005.04.002.

Haase, K. M., T. J. Worthington, P. Stoffers, C.-D. Garbe-Schonberg, and I. C. Write (2002), Mantle dynamics, element recycling and magma genesis beneath the Kermadec Arc-Havre Trough, *Geochem. Geophys. Geosyst.*, *3*(11), 1071, doi:10.1029/2002GC000335.

Hacker, B. R. (2008), H_2O subduction beyond arcs, *Geochem. Geophys. Geosyst.*, *9*, Q03001, doi:10.1029/2007GC001707.

Hacker, B. R., G. A. Abers, and S. M. Peacock (2003), Subduction factory 1. Theoretical mineralogy, densities, seismic wave speeds, and H_2O contents, *J. Geophys. Res.*, *108*(B1), 2029, doi:10.1029/2001JB001127.

Hauri, E. H., G. A. Gaetani, and T. H. Green (2006), Partitioning of water during melting of the Earth's upper mantle at H_2O-undersaturated conditions, *Earth Planet. Sci. Lett.*, *248*, 715–734, doi:10.1016/j.epsl.2006.06.014.

Hawkins, J. W., Jr., P. F. Lonsdale, J. D. MacDougall, and A. M. Volpe (1990), Petrology of the axial ridge of the Mariana Trough backarc spreading center, *Earth Planet. Sci. Lett.*, *100*, 226–250, doi:10.1016/0012-821X(90)90187-3.

Helsel, D. R., and R. M. Hirsch (2002), *Statistical methods in water resources: Techniques of Water-Resources Investigations of the United State Geological Survey*, Book 4, pp. 266–274, U.S. Geol. Surv., Reston, Va.

Hermann, J., and D. Rubatto (2009), Accessory phase control on the trace element signature of sediment melts in subduction zones, *Chem. Geol.*, *265*, 512–526, doi:10.1016/j.chemgeo.2009.05.018.

Hermann, J., and C. J. Spandler (2008), Sediment melts at sub-arc depths: An experimental study, *J. Petrol.*, *49*(4), 717–740, doi:10.1093/petrology/egm073.

Hermann, J., C. Spandler, A. Hack, and A. V. Korsakov (2006), Aqueous fluids and hydrous melts in high-pressure and ultra-high pressure rocks: Implications for element transfer in subduction zones, *Lithos*, *92*, 399–417, doi:10.1016/j.lithos.2006.03.055.

Hildreth, W. (2007), Quaternary magmatism in the Cascades—Geologic perspectives, *U.S. Geol. Surv. Prof. Pap.*, *1744*.

Hilton, D. R., T. P. Fischer, and B. Marty (2002), Noble gases and volatile recycling at subduction zones, *Rev. Mineral. Geochem.*, *47*(1), 319–370, doi:10.2138/rmg.2002.47.9.

Hirschmann, M. M. (2000), Mantle solidus: Experimental constraints and the effects of peridotite composition, *Geochem. Geophys. Geosyst.*, *1*(10), 1042, doi:10.1029/2000GC000070.

Hurwitz, S., R. H. Mariner, U. Fehn, and G. T. Snyder (2005), Systematics of halogen elements and their radioisotopes in thermal springs of the Cascade Range, Central Oregon, Western USA, *Earth Planet. Sci. Lett.*, *235*, 700–714, doi:10.1016/j.epsl.2005.04.029.

Ingebritsen, S. E., D. R. Sherrod, and R. H. Mariner (1989), Heat flow and hydrothermal circulation in the Cascade Range, North-Central Oregon, *Science*, *243*, 1458–1462, doi:10.1126/science.243.4897.1458.

Ito, E., D. M. Harris, and A. T. Anderson (1983), Alteration of oceanic crust and geologic cycling of chlorine and water, *Geochim. Cosmochim. Acta*, *47*, 1613– 1624.

Ivandic, M., I. Grevemeyer, A. Berhorst, E. R. Flueh, and K. McIntosh (2008), Impact of bending related faulting on the seismic properties of the incoming oceanic plate offshore of Nicaragua, *J. Geophys. Res.*, *113*, B05410, doi:10.1029/2007JB005291.

James, E. R., M. Manga, and T. P. Rose (1999), CO_2 degassing in the Oregon Cascades, *Geology*, *27*(9), 823–826, doi:10.1130/0091-7613(1999)027<0823:CDITOC>2.3.CO;2.

Jarrard, R. D. (2003), Subduction fluxes of water, carbon dioxide, chlorine, and potassium, *Geochem. Geophys. Geosyst.*, *4*(5), 8905, doi:10.1029/2002GC000392.

Jicha, B. R., B. S. Singer, J. G. Brophy, J. H. Fournelle, M. Johnson Clark, B. M. Beard, T. J. Lapen, and N. J. Mahlen (2004), Variable impact of the subducted slab on Aleutian island arc magma sources: Evidence from Sr, Nd, Pb, and Hf isotopes and trace element abundances, *J. Petrol.*, *45*, 1845–1875, doi:10.1093/petrology/egh036.

Johnson, E. R., P. J. Wallace, H. Delgado Granados, V. C. Manea, A. J. R. Kent, I. N. Bindeman, and C. S. Donegan (2009), Subduction-related volatile recycling and magma generation beneath Central Mexico: Insights from melt inclusions, oxygen isotopes and geodynamic models, *J. Petrol.*, *50*(9), 1729–1764, doi:10.1093/petrology/egp051.

Johnson, K. E., R. S. Harmon, J. M. Richardson, S. Moorbath, and D. F. Strong (1996), Isotope and trace element geochemistry of Augustine volcano, Alaska: Implications for magmatic evolution, *J. Petrol.*, *37*, 95–115, doi:10.1093/petrology/37.1.95.

Kay, R. W. (1978), Aleutian magnesian andesites: Melts from subduction Pacific ocean crust, *J. Volcanol. Geotherm. Res.*, *4*(1–2), 117–132, doi:10.1016/0377-0273(78)90032-X.

Kelley, K. A., and E. Cottrell (2009), Water and the oxidation state of subduction zone magmas, *Science*, *325*(5940), 605–607, doi:10.1126/science.1174156.

Kelley, K. A., T. Plank, J. Ludden, and H. Staudigel (2003), Composition of altered oceanic crust at ODP Sites 801 and 1149, *Geochem. Geophys. Geosyst.*, *4*(6), 8910, doi:10.1029/2002GC000435.

Kelley, K. A., T. Plank, T. L. Grove, E. M. Stolper, S. Newman, and E. Hauri (2006), Mantle melting as a function of water content beneath back-arc basins, *J. Geophys. Res.*, *111*, B09208, doi:10.1029/2005JB003732.

Kelley, K. A., T. Plank, S. Newman, E. M. Stolper, T. L. Grove, S. Parman, and E. H. Hauri (2010), Mantle melting as a function of water content beneath the Mariana arc, *J. Petrol.*, *51*, 1711–1738, doi:10.1093/petrology/egq036.

Kent, A. J. R., and T. R. Elliott (2002), Melt inclusions from Marianas arc lavas: Implications for the composition and formation of island arc magmas, *Chem. Geol.*, *183*, 263–286, doi:10.1016/S0009-2541(01)00378-3.

Kent, A. J. R., M. D. Norman, I. D. Hutcheon, and E. M. Stolper (1999), Assimilation of seawater-derived components in an oceanic volcano: Evidence from matrix glasses and glass inclusions from Loihi seamount, Hawaii, *Chem. Geol.*, *156*, 299–319, doi:10.1016/S0009-2541(98)00188-0.

Kessel, R., M. W. Schmidt, P. Ulmer, and T. Pettke (2005), Trace element signature of subduction-zone fluids, melts and supercritical liquids at 120–180 km depth, *Nature*, *437*, 724–727, doi:10.1038/nature03971.

Kirby, S. H., S. Stein, E. A. Okal, and D. C. Rubie (1996), Metastable mantle phase transformations and deep earthquakes in subducting oceanic lithosphere, *Rev. Geophys.*, *34*, 261–306, doi:10.1029/96RG01050.

Klimm, K., J. D. Blundy, and T. H. Green (2008), Trace element partitioning and accessory phase saturation during H_2O-saturated melting of basalt with implications for subduction zone chemical fluxes, *J. Petrol.*, *49*(3), 523–553, doi:10.1093/petrology/egn001.

Kopp, H., et al. (2011), Deep structure of the central Lesser Antilles Island Arc: Relevance for the formation of continental crust, *Earth Planet. Sci. Lett.*, *304*(1–2), 121–134, doi:10.1016/j.epsl.2011.01.024.

Lee, C. A., P. Luffi, T. Plank, H. Dalton, and W. P. Leeman (2009), Constraints on the depths and temperatures of basaltic magma generation on Earth and other terrestrial planets using new thermobarometers for mafic magmas, *Earth Planet. Sci. Lett.*, *279*, 20–33, doi:10.1016/j.epsl.2008.12.020.

Leeman, W. P. (1996), Boron and other fluid-mobile elements in volcanic arc lavas: Implications for subduction processes, in *Subduction Top to Bottom*, *Geophys. Monogr. Ser.*, vol. 96, edited by E. Bebout et al., pp. 269–276, AGU, Washington, D. C., doi:10.1029/GM096p0269.

Leeman, W. P., D. R. Smith, W. Hildreth, Z. Palacz, and N. Rogers (1990), Compositional diversity of Late Cenozoic basalts in a transect across the Southern Washington Cascades: Implications for subduction zone magmatism, *J. Geophys. Res.*, *95*(B12), 19,561–19,582, doi:10.1029/JB095iB12p19561.

Le Roux, P. J., S. B. Shirey, E. H. Hauri, M. R. Perfit, and J. F. Bender (2006), The effects of variable sources, processes and contaminants on the composition of northern EPR MORB (8–10°N and 12–14°N): Evidence from volatiles (H_2O, CO_2, S) and halogens (F, Cl), *Earth Planet. Sci. Lett.*, *251*, 209–231, doi:10.1016/j.epsl.2006.09.012.

Levin, V., J. Park, M. Brandon, J. Lees, V. Peyton, E. Gordeev, and A. Ozerov (2002), Crust and upper mantle of Kamchatka from teleseismic receiver functions, *Tectonophysics*, *358*, 233–265, doi:10.1016/S0040-1951(02)00426-2.

Le Voyer, M., E. F. Rose-Koga, N. Shimizu, T. L. Grove, and P. Schiano (2010), Two contrasting H_2O-rich components in primary melt inclusions from Mount Shasta, *J. Petrol.*, *51*(7), 1571–1595, doi:10.1093/petrology/egq030.

Mangan, M. T., T. P. Miller, C. F. Waythomas, F. A. Trusdell, A. T. Calvert, and P. W. Layer (2009), Diverse lavas from closely spaced volcanoes drawing from a common parent: Emmons Lake Volcanic Center, Eastern Aleutian Arc, *Earth Planet. Sci. Lett.*, *287*, 363–372, doi:10.1016/j.epsl.2009.08.018.

Manning, C. E. (2004), The chemistry of subduction-zone fluids, *Earth Planet. Sci. Lett.*, *223*, 1–16, doi:10.1016/j.epsl.2004.04.030.

Marsh, B. D. (1982), The Aleutians, in *Orogenic Andesites*, pp. 99–114, John Wiley, Chichester, U. K.

Martin, E., I. Bindeman, and T. L. Grove (2011), The origin of high-Mg magmas in the Mt. Shasta and Medicine Lake volcanoes, Cascade Arc (California): Higher and lower than mantle oxygen isotope signatures attributed to current and past subduction, *Contrib. Mineral. Petrol.*, *162*(5), 945–960, doi:10.1007/s00410-011-0633-4.

McDonough, W. F., and S.-S. Sun (1995), Composition of the Earth, *Chem. Geol.*, *120*, 223–253, doi:10.1016/0009-2541(94)00140-4.

Metrich, N., and P. J. Wallace (2008), *Volatile Abundances in Basaltic Magmas and Their Degassing Paths Tracked by Melt Inclusions*, *Rev. Mineral.*, vol. 69, edited by K. D. Putirka and F. J. Tepley III, pp. 363–402, Mineral. Soc. of Am., Chantilly, Va.

Miller, D. M., C. H. Langmuir, S. L. Goldstein, and A. L. Franks (1992), The importance of parental magma composition to calc-alkaline and tholeiitic evolution: Evidence from Umnak Island in the Aleutians, *J. Geophys. Res.*, *97*(B1), 321–343, doi:10.1029/91JB02150.

Miller, M. M., D. J. Johnson, C. M. Rubin, H. Dragert, K. Wang, A. Qamar, and C. Goldfinger (2001), GPS-determination of along-strike variation in Cascadia margin kinematics: Implications for relative plate motion, subduction zone coupling, and permanent deformation, *Tectonics*, *20*(2), 161–176, doi:10.1029/2000TC001224.

Myers, J. D., B. D. Marsh, C. D. Frost, and J. A. Linton (2002), Petrologic constraints on the spatial distribution of crustal magma chambers, Atka Volcanic Center, Central Aleutian Arc, *Contrib. Mineral. Petrol.*, *143*, 567–586, doi:10.1007/s00410-002-0356-7.

Newman, S., E. M. Stolper, and R. J. Stern (2000), H_2O and CO_2 in magmas from the Mariana arc and back arc systems, *Geochem. Geophys. Geosyst.*, *1*(5), 1013, doi:10.1029/1999GC000027.

Nye, C. J., and M. R. Reid (1986), Geochemistry of primary and least fractionated lavas from Okmok Volcano, Central Aleutians: Implications for arc magmagenesis, *J. Geophys. Res.*, *91*, 10,271–10,287, doi:10.1029/JB091iB10p10271.

Parman, S. W., and T. L. Grove (2004), Harzburgite melting with and without H_2O: Experimental data and predictive modeling, *J. Geophys. Res.*, *109*, B02201, doi:10.1029/2003JB002566.

Peacock, S. M. (2003), Thermal structure and metamorphic evolution of subducting slabs, in *Inside the Subduction Factory*, *Geophys. Monogr. Ser.*, vol. 138, edited by J. Eiler, pp. 7–22, AGU, Washington, D. C., doi:10.1029/138GM02.

Pearce, J. A., and D. W. Peate (1995), Tectonic implications of the composition of volcanic arc magmas, *Annu. Rev. Earth Planet. Sci.*, *23*, 251–285, doi:10.1146/annurev.ea.23.050195.001343.

Plank, T., and C. H. Langmuir (1988), An evaluation of the global variations in the major element chemistry of arc basalts, *Earth Planet. Sci. Lett.*, *90*, 349–370, doi:10.1016/0012-821X(88)90135-5.

Plank, T., and C. H. Langmuir (1993), Tracing trace elements from sediment input to volcanic output at subduction zones, *Nature*, *362*, 739–743, doi:10.1038/362739a0.

Plank, T., and C. H. Langmuir (1998), The chemical composition of subducting sediment and its consequences for the crust and mantle, *Chem. Geol.*, *145*, 325–394, doi:10.1016/S0009-2541(97)00150-2.

Plank, T., V. Balzer, and M. Carr (2002), Nicaraguan volcanoes record paleoceanographic changes accompanying closure of the Panama gateway, *Geology*, *30*(12), 1087–1090, doi:10.1130/0091-7613(2002)030<1087:NVRPCA>2.0.CO;2.

Plank, T., L. B. Cooper, and C. E. Manning (2009), Emerging geothermometers for estimating slab surface temperatures, *Nat. Geosci.*, *2*, 611–615, doi:10.1038/ngeo614.

Ponomareva, V., I. Melekestsev, O. Braitseva, T. Churikova, M. Pevzner, and L. Sulerzhitsky (2007), Late Pleistocene-Holocene volcanism on the Kamchatka Peninsula, Northwest Pacific Region, in *Volcanism and Subduction: The Kamchatka Region*, *Geophys. Monogr. Ser.*, vol. 172, edited by J. Eichelberger et al., pp. 165–198, AGU, Washington, D. C., doi:10.1029/172GM15.

Portnyagin, M., K. Hoernle, P. Plechov, N. Mironov, and S. Khbunaya (2007), Constraints on mantle melting and composition and nature of slab components in volcanic arcs from volatiles (H_2O, S, Cl, F) and trace elements in melt inclusions from the Kamchatka Arc, *Earth Planet. Sci. Lett.*, *255*, 53–69, doi:10.1016/j.epsl.2006.12.005.

Ranero, C. R., J. Phipps Morgan, K. McIntosh, and C. Reichert (2003), Bending, faulting, and mantle serpentinization at the Middle America Trench, *Nature*, *425*, 367–373, doi:10.1038/nature01961.

Reiners, P. W., P. E. Hammond, J. M. McKenna, and R. A. Duncan (2000), Young basalts of the central Washington Cascades, flux melting of the mantle, and trace element signatures of primary arc magmas, *Contrib. Mineral. Petrol.*, *138*, 249–264.

Roberge, J., H. Delgado-Granados, and P. J. Wallace (2009), Mafic magma recharge supplies high CO_2 and SO_2 gas fluxes from Popocatepetl volcano, Mexico, *Geology*, *37*(2), 107–110, doi:10.1130/G25242A.1.

Roggensack, K. (2001), Unraveling the 1974 eruption of Fuego volcano (Guatemala) with small crystals and their young melt inclusions, *Geology*, *29*(10), 911–914, doi:10.1130/0091-7613(2001)029<0911:UTEOFV>2.0.CO;2.

Roggensack, K., R. L. Hervig, S. B. McKnight, and S. N. Williams (1997), Explosive basaltic volcanism from Cerro Negro Volcano: Influence of volatiles on eruptive style, *Science*, *277*, 1639–1642, doi:10.1126/science.277.5332.1639.

Romick, J. D., M. R. Perfit, S. E. Swanson, and R. D. Shuster (1990), Magmatism in the Eastern Aleutian arc: Temporal characteristic of igneous activity on Akutan Island, *Contrib. Mineral. Petrol.*, *104*, 700–721, doi:10.1007/BF01167288.

Rowe, M. C., A. J. R. Kent, and R. L. Nielsen (2007), Determination of sulfur speciation and oxidation state of olivine hosted melt inclusions, *Chem. Geol.*, *236*, 303–322, doi:10.1016/j.chemgeo.2006.10.007.

Rowe, M. C., A. J. R. Kent, and R. L. Nielsen (2009), Subduction influence on oxygen fugacity and trace and volatile elements in basalts across the Cascades volcanic arc, *J. Petrol.*, *50*(1), 61–91, doi:10.1093/petrology/egn072.

Ruscitto, D. M., P. J. Wallace, E. R. Johnson, A. J. R. Kent, and I. N. Bindeman (2010), Volatile contents of mafic magmas from cinder cones in the Central Oregon High Cascades: Implications for magma formation and mantle conditions in a hot arc, *Earth Planet. Sci. Lett.*, *298*, 153–161, doi:10.1016/j.epsl.2010.07.037.

Ruscitto, D. M., P. J. Wallace, and A. J. R. Kent (2011), Revisiting the compositions and volatile contents of olivine-hosted melt inclusions from the Mount Shasta region: Implications for the formation of high-Mg andesites, *Contrib. Mineral. Petrol.*, *162*(1), 109–132, doi:10.1007/s00410-010-0587-y.

Ryan, J. G., and C. H. Langmuir (1993), The systematics of boron abundances in young volcanic rocks, *Geochim. Cosmochim. Acta*, *57*, 1489–1498, doi:10.1016/0016-7037(93)90008-K.

Sadofsky, S. J., M. Portnyagin, K. Hoernle, and P. van den Bogaard (2008), Subduction cycling of volatiles and trace elements through the Central American volcanic arc: Evidence from melt inclusions, *Contrib. Mineral. Petrol.*, *155*, 433–456, doi:10.1007/s00410-007-0251-3.

Saito, G., Y. Morishita, and H. Shinohara (2010), Magma plumbing system of the 2000 eruption of Miyakejima volcano, Japan, deduced from volatile and major component contents of olivine-hosted melt inclusions, *J. Geophys. Res.*, *115*, B11202, doi:10.1029/2010JB007433.

Schmidt, M. W., and S. Poli (1998), Experimentally based water budgets for dehydrating slabs and consequences for arc magma generation, *Earth Planet. Sci. Lett.*, *163*, 361–379, doi:10.1016/S0012-821X(98)00142-3.

Shaw, A. M., E. H. Hauri, T. P. Fischer, D. R. Hilton, and K. A. Kelley (2008), Hydrogen isotopes in Mariana arc melt inclusions: Implications for subduction dehydration and the deep-Earth water cycle, *Earth Planet. Sci. Lett.*, *275*, 138–145, doi:10.1016/j.epsl.2008.08.015.

Sherrod, D. R., and J. G. Smith (1990), Quaternary extrusion rates of the Cascade Range, Northwestern United States and Southern British Columbia, *J. Geophys. Res.*, *95*(B12), 19,465–19,474, doi:10.1029/JB095iB12p19465.

Shillington, D. J., H. J. A. Van Avendonk, W. S. Holbrook, P. B. Kelemen, and M. J. Hornbach (2004), Composition and structure of the central Aleutian island arc from arc-parallel wide-angle seismic data, *Geochem. Geophys. Geosyst.*, *5*, Q10006, doi:10.1029/2004GC000715.

Singer, B. S., B. R. Jicha, W. P. Leeman, N. W. Rogers, M. F. Thirlwall, J. Ryan, and K. E. Nicolaysen (2007), Along-strike trace element and isotopic variation in Aleutian Island arc basalt: Subduction melts sediments and dehydrates serpentine, *J. Geophys. Res.*, *112*, B06206, doi:10.1029/2006JB004897.

Sisson, T. W., and S. Bronto (1998), Evidence for pressure-release melting beneath magmatic arcs from basalt at Galunggung, Indonesia, *Nature*, *391*, 883–886, doi:10.1038/36087.

Sisson, T. W., and G. D. Layne (1993), H_2O in basalt and basaltic andesite glass inclusions from four subduction-related volcanoes, *Earth Planet. Sci. Lett.*, *117*, 619–635, doi:10.1016/0012-821X(93)90107-K.

Stolper, E., and S. Newman (1994), The role of water in the petrogenesis of Mariana Trough magmas, *Earth Planet. Sci. Lett.*, *121*, 293–325, doi:10.1016/0012-821X(94)90074-4.

Sun, S.-S., and W. F. McDonough (1989), Chemical and isotopic systematics of oceanic basalts: implications for mantle composition and processes, in *Magmatism in the Ocean Basins*, edited by A. D. Saunders and M. J. Norry, *Spec. Publ. Geol. Soc.*, 42, 313–345.

Syracuse, E. M., and G. A. Abers (2006), Global compilation of variations in slab depth beneath arc volcanoes and implications, *Geochem. Geophys. Geosyst.*, *7*, Q05017, doi:10.1029/2005GC001045.

Syracuse, E. M., P. E. van Keken, and G. A. Abers (2010), The global range of subduction zone thermal models, *Phys. Earth Planet. Inter.*, *183*(1–2), 73–90, doi:10.1016/j.pepi.2010.02.004.

Takahashi, N., S. Kodaira, S. L. Klemperer, Y. Tatsumi, Y. Kaneda, and K. Suyehiro (2007), Crustal structure and evolution of the Mariana intra-oceanic island arc, *Geology*, *35*(3), 203–206, doi:10.1130/G23212A.1.

Taran, Y. A. (2009), Geochemistry of volcanic and hydrothermal fluids and volatile budget of the Kamchatka-Kuril subduction zone, *Geochim. Cosmochim. Acta*, *73*, 1067–1094, doi:10.1016/j.gca.2008.11.020.

Tolstykh, M. L., V. B. Naumov, A. D. Babansky, G. E. Bogoyavlenskaya, and S. Khubunaya (2003), Chemical composition, volatile components, and trace elements in andesitic magmas of the Kurile-Kamchatka region, *Petrology*, *16*(1), 1–18, doi:10.1134/S0869591108010013.

van Keken, P. E., B. R. Hacker, E. M. Syracuse, and G. A. Abers (2011), Subduction factory: 4. Depth-dependent flux of H_2O from subducting slabs worldwide, *J. Geophys. Res.*, *116*, B01401, doi:10.1029/2010JB007922.

Wade, J. A., T. Plank, W. G. Melson, G. J. Soto, and E. H. Hauri (2006), The volatile content of magmas from Arenal volcano, Costa Rica, *J. Volcanol. Geotherm. Res.*, *157*, 94–120, doi:10.1016/j.jvolgeores.2006.03.045.

Walker, J. A., K. Roggensack, L. C. Patino, B. I. Cameron, and O. Matias (2003), The water and trace element contents of melt inclusions across an active subduction zone, *Contrib. Mineral. Petrol.*, *146*, 62–77, doi:10.1007/s00410-003-0482-x.

Wallace, P. J. (2005), Volatiles in subduction zone magmas: Concentrations and fluxes based on melt inclusion and volcanic gas data, *J. Volcanol. Geotherm. Res.*, *140*, 217–240, doi:10.1016/j.jvolgeores.2004.07.023.

Wallace, P. J., and I. S. E. Carmichael (1992), Sulfur in basaltic magmas, *Geochim. Cosmochim. Acta*, *56*(5), 1863–1874, doi:10.1016/0016-7037(92)90316-B.

Wallace, P. J., and I. S. E. Carmichael (1999), Quaternary volcanism near the Valley of Mexico: Implications for subduction zone magmatism and the effects of crustal thickness variations on primitive magma compositions, *Contrib. Mineral. Petrol.*, *135*, 291–314, doi:10.1007/s004100050513.

Wasylenki, L. E., M. B. Baker, A. J. R. Kent, and E. M. Stolper (2003), Near-solidus melting of the shallow upper mantle: Partial melting experiments on depleted peridotite, *J. Petrol.*, *44*(7), 1163–1191, doi:10.1093/petrology/44.7.1163.

White, S. M., J. A. Crisp, and F. J. Spera (2006), Long-term volumetric eruption rates and magma budgets, *Geochem. Geophys. Geosyst.*, *7*, Q03010, doi:10.1029/2005GC001002.

Wilson, D. S. (2002), The Juan de Fuca plate and slab: Isochron structure and Cenozoic plate motions, in *The Cascadia Subduction Zone and Related Subduction Systems*, edited by S. Kirby, K. Wang, and S. Dunlop, *U.S. Geol. Surv. Open File Rep.*, *02–328*, 9–12.

Wysoczanski, R., and K. Tani (2006), Spectroscopic FTIR imaging of water species in silicic volcanic glasses and melt inclusions: An example from the Izu-Bonin arc, *J. Volcanol. Geotherm. Res.*, *156*(3–4), 302–314, doi:10.1016/j.jvolgeores.2006.03.024.

Zimmer, M. M., T. Plank, E. H. Hauri, G. M. Yogodzinski, P. Stelling, J. Larsen, B. S. Singer, B. R. Jicha, C. W. Mandeville, and C. J. Nye (2010), The role of water in generating the calc-alkaline trend: New volatile data for Aleutian magmas and a new Tholeiitic Index, *J. Petrol.*, *51*, 2411–2444, doi:10.1093/petrology/egq062.

Supplemental Material 1: Data Sources and Treatment

For some volcanoes, we used published values of primitive magma compositions that had been constructed from melt inclusion data using the same method we use here (e.g., Portnyagin et al., 2007; Johnson et al., 2009; Kelley et al., 2010). Complete compositional datasets (major, volatile, and trace analyses) for melt inclusions are not available for all volcanoes, and our data set was therefore augmented with whole rock data and glass analyses of similar compositions from the same vent. All calculations were performed under the conditions (f_{O2}, Fe-Mg K_D, mantle Fo content) specified by the authors of each data set. If no conditions were specified, compositions were restored to equilibrium with Fo_{90} olivine at NNO ($Fe^{2+}/Fe^{Total} \sim 0.80$) using K_D=0.30. All melt components, other than MgO, FeO and SiO_2, were diluted during the restoration process (i.e., $D^{solid\text{-}melt} = 0$). Primitive magma volatile contents were determined by taking the maximum H_2O and average S and Cl contents from the least degassed inclusions. Average S and Cl contents were used, rather than maxima, because these components tend to degas at shallower pressures than H_2O (Spilliaert et al., 2006; Johnson et al., 2010). Available B data (predominantly from whole rocks) were also compiled from sources listed in Table 1 and below. CO_2 contents from melt inclusions were used only to constrain least-degassed samples; primitive melt CO_2 values were not calculated because the extremely low solubility of CO_2 in silicate melts leads to substantial degassing prior to melt inclusion formation (Wallace, 2005; Blundy & Cashman, 2010). Primitive melt volatile and B contents were diluted by the appropriate amount of olivine addition required for mantle equilibration. Full primitive magma compositions are tabulated in Supplemental Material 2. Note that we have used 4.3 wt.% H_2O (C. Mandeville, personal communication 2011) for the primary magmatic value of the Galunggung magma (Table 1) even though this magma was interpreted to reflect decompression-related melting (rather than fluid flux melting) by Sisson & Bronto (1998). The low reported H_2O values likely reflect diffusive H_2O loss because the inclusions were from volcanic bombs, which have been shown to cool slowly enough to permit significant loss of H_2O from olivine-hosted melt inclusions (Lloyd et al., 2010); moreover, S and Cl contents are relatively high in the Galunggung melt inclusions (0.14 and 0.11 wt.%, respectively), similar to other arc magmas (Fig. 4a, b,c; 5a, b, d; Table 1; Massare et al., 2002; Portnyagin et al., 2008).

Based on analytical uncertainties, reported magmatic H_2O contents should be accurate to within 10% while S, Cl, and B contents should be accurate to within 3-5% (cf., Shaw et al., 2008; Ruscitto et al., 2010, 2011). The dominant contributions to uncertainty in the total extent of crystallization are derived from Fe-Mg K_D ratios, the oxidation state of the magma, and the crystallization of phases other than olivine (e.g., pyroxene, amphibole, plagioclase). Using the average Central Cascades composition as an example (~18 wt.% olivine added for equilibration with Fo_{90}), the uncertainty in the olivine-melt Fe-Mg K_D ratio (i.e., varying K_D from 0.27 to 0.33; 0.30 ±0.03) translates into differences of ±5-6 wt.% in calculated amounts of incremental olivine addition required to bring melt compositions into equilibrium with the mantle (e.g., Fo_{90}). Increasing (or decreasing) the assumed oxidation state of the magma by one log unit (i.e., NNO ±1) also results in the decrease (or increase) of calculated olivine addition by 5-6 wt.%. We consider it unlikely that our assumed values for Fe-Mg K_D and oxidation state

are offset by more than the amounts provided in the example, and so our estimated amount of olivine addition for this composition is 18 ±8.5 wt.%. For most elements (not incorporated into olivine), this corresponds to a dilution factor of 1.18 ±0.085 or ~7% maximum uncertainty. The crystallization of minerals other than olivine may be important, particularly in the deep crust, however we are currently unable to quantify the uncertainty related to the crystallization of phases other than olivine but we make this point for completeness. Combining the analytical uncertainty with that from the extent of crystallization, we estimate that the absolute concentrations of volatile contents in the primitive magmas reported in Table 1 should be accurate to within ~10-12%. Uncertainties in volatile/elemental ratios for the magmas should be considerably less assuming that the components do not to fractionate from one another during crystallization and that these primitive melts represent undegassed samples.

Data Sources:

1. *Southern Cascades:* Goosenest, Copco, and Black Crater MI data are from Sisson & Layne (1993), parent melt compositions were calculated for this study. Shasta high-Mg andesite (HMA) and primitive basaltic andesite (PBA) of MI (and preferred parent compositions) are from the S17 cinder cone in Ruscitto et al. (2011). Oxygen isotope data are from Martin et al. (2011).

2. *Central Cascades:* MI data, parent compositions, and olivine oxygen isotopes for Sand Mountain, Twin Craters, Island Fissure, Collier Cone, Yapoah, Blue Lake Maar, and Garrison Butte are from Ruscitto et al. (2010). Additional unpublished MI analyses (Ruscitto, 2011) for Four-in-One and Collier Cone are included. Samples CC021, BC021, DB042, BR022, KWB031, BB031, LTB022, AIC021, ELK021, TB021, and SIC021 are from MI data in Rowe et al. (2009). H_2O contents (at Fo_{90}) for Rowe samples were determined by interpolation using linear relationships between measured H_2O, TiO_2, Er, and Yb contents in the Ruscitto data. B data for Southern WA Cascades are from Leeman et al. (2004).

3. *Chichinautzin Volcanic Field:* Jumiltepec, Las Tetillas, Tepetlapa, Xitle, and Tuxtepec MI data are from Cervantes & Wallace (2003). Popocatepetl MI from Roberge et al. (2009). Parent melt compositions were calculated for this study. B data from Straub et al. (2008).

4. *Michoacan-Guanajuato Volcanic Field:* All MI data, parental melt compositions, and olivine oxygen isotopes come from Johnson et al. (2009).

5. *Guatemala/El Salvador:* MI data for Fuego are from Sisson & Layne (1993) and Roggensack (2001). MI data for La Providencia, Cerro Mongoy, Cerro Ovejero, and Cerro Las Ruidas are from Walker et al. (2003). Parental melt compositions were calculated for this study from the above MI data. Tabulated parent melt compositions (equilibrium with Fo_{91}) for Atitlan, Santa Maria, Fuego, and Agua come from Sadofsky et al. (2008). B data from Leeman et al. (1994). Oxygen isotopes from Eiler et al. (2005).

6. *Costa Rica:* MI data for Arenal (Wade et al., 2006) and Irazu (Benjamin et al., 2007) were used to construct parent melt compositions and were averaged with parent melt compositions reported by Sadofsky et al. (2008). B data from Leeman et al. (1994). Oxygen isotopes from Eiler et al. (2005).

7. *Southern Lesser Antilles:* MI data from Grenada (Bouvier et al., 2008) and St. Vincent (Bouvier et al., 2010) were used to construct parent melt compositions for this study.

8. *Nicaragua:* MI data for Cerro Negro (Roggensack, 2001) were used to calculate a parental melt composition and was averaged with the composition specified in Sadofsky et al. (2008). Other parent melt compositions used from Sadofsky et al. (2008) for Nejapa and Granada (high and low Nb-types). B data from Leeman et al. (1994). Oxygen isotopes from Eiler et al. (2005).

9. *Alaska (Augustine):* MI data from Zimmer et al. (2010). WR trace element data from Johnson et al. (1996).

10. *Eastern Aleutians:* All MI data (olivine-hosted only) from Zimmer et al. (2010). WR trace elements for Okmok (Nye & Reid, 1986; Miller et al., 1992), Akutan (Romick et al., 1990), Unalaska Island (George et al., 2003; Singer et al., 2007), Shishaldin (Jicha et al., 2004), and Emmons (Mangan et al., 2009). B data from Singer et al. (2007).

11. *Central Aleutians:* All MI data (olivine-hosted only) from Zimmer et al. (2010). WR trace elements for Korovin (Marsh, 1982; Myers et al., 2002) and Seguam (Jicha et al., 2004). B data from Singer et al. (2007).

12. *Izu-Bonin Arc, Miyakejima*: MI data from Saito et al. (2010). No trace element data.

13. *Kamchatka:* MI data from Klyuchevskoy (Auer et al., 2009) were used to calculate a parent melt composition and then averaged with specified parent compositions from Portnyagin et al. (2007). Parent melt compositions for Ksudach, Karymsky, , Tolbachik, and Farafonova Pad from Portnyagin et al. (2007). Oxygen isotopes for Klyuchevskoy from Auer et al. (2009).

14. *Java:* MI data for Galunggung from Sisson & Bronto (1998). Primitive melt composition for Kawah Ijen provided by Nathalie Vigouroux.

15. *Southern Kurile Arc:* MI data for Kudryavy M.I. from Tolstykh et al., 2003 (no H_2O data).

16. *Northern Kurile Arc*: MI data for Chikurachki (Gurenko et al., 2005) used to calculate parent melt composition and averaged with the tabulated composition in Portnyagin et al. (2007).

17. *Marianas:* MI data (volatiles and oxides) for Agrigan (Newman et al., 2000; Shaw et al., 2008; Kelley et al., 2010), Guguan (Shaw et al., 2008; Kelley et al., 2010), Pagan (Shaw et al., 2008; Kelley et al., 2010), Sarigan (Shaw et al., 2008; Kelley et al., 2010), Asuncion and Alamagan (both from Shaw et al.,2008), were used to independently calculate parent melt compositions, which were subsequently averaged for each volcano. Parent melt trace element contents for Agrigan and Guguan were calculated using MI data from Kent & Elliot (2002). Parent melt trace element contents for Alamagan, Sarigan, Pagan, and Asuncion calculated from WR data from Elliot et al. (1997). B (and Nb, La) WR data for Sarigan, Guguan, Alamagan, Pagan, Agrigan, and Asuncion from Ishikawa & Tera (1983) and Woodhead (1989). Oxygen isotopes from Eiler et al. (2000).

18. *Tonga*: MI data (volatiles, oxides) and GL (trace elements) for Volcano A (Cooper et al., 2010). MI and GL data for L, D, F, 7, 19, and Tofua from Cooper (2009). Note that MI from Volcano F are in plagioclase and MI from Tofua are from olivine, plagioclase and clinopyroxene. B data from George et al. (2005).

Back-arc Basin Basalts:
Marianas Trough: H_2O contents for ridge segments 15-17 ºN, 17-19 ºN, and 19-21 ºN are from Kelley et al. (2006). GL data (volatiles, oxides) for sample WOKD28-3 (Newman et al., 2000; Stolper & Newman, 1994) was augmented with trace elements from basalts with > 6 wt.% MgO (Hawkins, 1990; Gribble, 1996). The average GL composition (volatiles, oxides, trace elements) of samples from Gribble et al. (1996) were averaged and used to calculate a parent melt composition.
Lau Basin: H_2O contents for ridge segments VFR, MTJ, ELSC, ILSC, and CLSC are from Kelley et al. (2006). High and low Nb/Zr GL data (volatiles, oxides, trace elements) from the Eastern Lau Spreading Center (ELSC) reported by Bezos et al. (2009) were used to calculate parent melt compositions.
East Scotia Ridge and Manus Basin: H_2O contents from Kelley et al. (2006).
Ngatoro Basin (S. Kermadec): GL data (volatiles, oxides) from Wysocanski et al. (2006).
Havre Trough (Kermadec): GL data (S, Cl, trace elements) from Haase et al. (2002).
Izu-Bonin: MI data (S, Cl, oxides) from Rowe et al. (2007).

Additional References (not cited in publication):

Johnson, E.R., Wallace, P.J., Cashman, K.V., Delgado Granados, H., 2010. Degassing of volatiles (H_2O, CO_2, S, Cl) during ascent, crystallization, and eruption at mafic monogenetic volcanoes in central Mexico. J. Volcanol. Geotherm. Res. 197: 225-238.

Lloyd, A.S., Plank, T., Ruprecht, P., Hauri, E.H., Rose, W.I., 2010. Volatile loss from melt inclusions in clasts of differing sizes. American Geophys. Union, Fall Meeting, abstract V24C-04.

Massare, D., N. Metrich, and R. Clocchiatti (2002) High-temperature experiments on silicate melt inclusions in olivine at 1 atm: inference on temperatures of homogenization and H_2O concentrations. Chem Geol, 183: 87-98.

Portnyagin, M., Almeev, R., Matveev, S., Holtz, F., 2008. Experimental evidence for rapid water exchange between melt inclusions in olivine and host magma. Earth Planet. Sci. Lett. 272: 541–552.

Spilliaert, N., Allard, P., Métrich, N., Sobolev, A.V., 2006. Melt inclusion record of the conditions of ascent, degassing, and extrusion of volatile-rich alkali basalt during the powerful 2002 flank eruption of Mount Etna (Italy). J. Geophys. Res. 111. doi:10.1029/2005JB003934.

Supplemental Material 3

A. Modeling of Subduction Components

Starting mantle compositions were assumed for each arc segment, and preferred compositions were used if specified in the original study (e.g., Eiler et al., 2005 [Central America]; Grove et al., 2002 [Southern Cascades/Shasta]; Portnyagin et al., 2007 [Kamchatka, N. Kurile]; Johnson et al., 2009 [CVF & MGVF Mexico]; Ruscitto et al., 2010 [Central Cascades], Kelley et al., 2010 [Marianas]). If no mantle composition was specified, either the depleted MORB source (DMM) of Salters & Stracke (2004) or the enriched DMM source (E-DMM) of Workman & Hart (2005) was assigned to an arc segment based on the relative enrichments in TiO_2 and Y contents in the parental magmas (c.f., Nb vs. Y in Portnyagin et al., 2007). An enriched mantle source appears to be required to adequately model Lesser Antilles magmas, but given the poor constraints on the composition of such a source, SCs were not calculated for this arc. The list of references used for modeling the mantle source compositions and bulk mineral-melt partition coefficients in each arc segment can be found in the table below. Uncertainties in calculated SCs were evaluated for the Central and Southern Cascades using a Monte Carlo approach (N=300) by allowing primitive magma compositions to vary within the 95% confidence interval. Calculated uncertainties do not include uncertainties in assumed mantle compositions or bulk partition coefficients, which could be considerable, but are useful for evaluating the variability of calculated SCs given uncertainties in the calculated degrees of melting. All model results and calculated SCs (along with 1 s.e. estimates for Cascades SCs) are reported in Table 2. Average uncertainties in F are ~1.4 % by Monte Carlo methods, this is smaller than the reported uncertainties in Table 2 which are determined by the misfit of HFSE elements after Portnyagin et al. (2007).

References for Mantle Compositions and Partition Coefficients

	Mantle Composition	Bulk D Source	Notes
1. Southern Cascades	Grove et al., 2002	after Johnson et al., 2009	6% Depleted Source (Ol: 65/Opx: 35/Cpx: 0/Spl: 0)
2. Central Cascades	Ruscitto et al., 2010	after Johnson et al., 2010	BLW Source (Ol: 53/Opx: 30/Cpx: 12/Spl: 5)
3. CVF	Workman & Hart, 2005	Workman & Hart, 2005	
5. Guat/El Salvador	Eiler et al., 2005	Eiler et al., 2005	
6. Costa Rica	Eiler et al., 2005	Eiler et al., 2005	
7. S. Lesser Antilles	Workman & Hart, 2005	Workman & Hart, 2005	
8. Nicaragua	Eiler et al., 2005	Eiler et al., 2005	
9. Alaska	Workman & Hart, 2005	Workman & Hart, 2005	
10. E. Aleutians	Workman & Hart, 2005	Workman & Hart, 2005	
11. C. Aleutians	Workman & Hart, 2005	Workman & Hart, 2005	
13. Kamchatka Arc	Workman & Hart, 2005	Workman & Hart, 2005	
14. Java	Workman & Hart, 2005	Workman & Hart, 2005	
16. North Kurile Arc	Workman & Hart, 2005	Workman & Hart, 2005	
17. Marianas Arc	Salters & Stracke, 2004	Kelley et al., 2006	
18. Tonga Arc	Salters & Stracke, 2004	Kelley et al., 2006	

B. Hydrous Melting in the Mantle Wedge

Average degrees of melting determined for the primitive compositions in Table 1 using the methods described in Section 4.2.1 are shown in Figure S1 along with magmatic and bulk mantle source H_2O contents. Hydrous melting curves in Figure S1 illustrate inferred relationships between the degrees of melting and the H_2O contents of mantle sources and resulting melts at given pressure and temperature conditions. These hydrous melting curves were calculated for each arc segment by combining the hydrous melting parameterization of Kelley et al. (2010) (their equation 4; DMM1 source) with the average temperatures and pressures determined for the primitive magma compositions after Lee et al. (2009) (Lee temperatures have been converted to $T - T_0$, where T_0 refers to the dry mantle solidus at a particular pressure; Kelley et al., 2010). Unreasonably high average temperature and pressure estimates of 1570 ±161 ºC and 4.7 ±1.9 GPa result from forcing the parameterization through the entire data set (r^2=0.62), indicating that a single set of mantle conditions is not appropriate for modeling magma generation beneath different arc segments. Rather, each arc (and likely each individual magma batch) reflects a particular set of conditions. (Section 2; Figure 3). Our results are broadly consistent with those found in previous studies and confirm that at a given degree of melting, arc magmas are produced under cooler melting conditions (e.g., more H_2O present) than MORB or BABB (Stolper & Newman, 1994; Kelley et al., 2006; Portnyagin, 2007; Johnson et al., 2009; Kelley et al., 2010; Ruscitto et al., 2010).

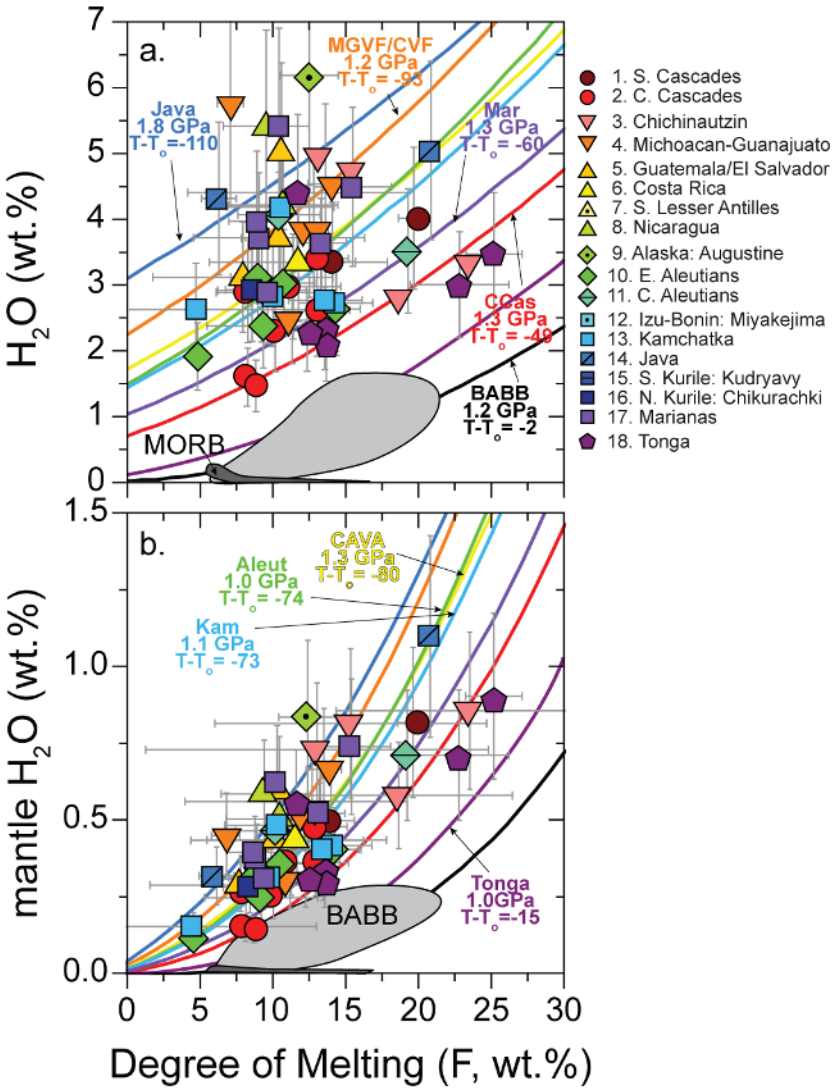

FIGURE S1. Magmatic H_2O contents (a) and corresponding source mantle H_2O contents (b) plotted against estimated degrees of modal batch melting for primitive arc magmas. Symbols are the same as in Figure 1 with fields shown for parental BABB and MORB melts (after Portnyagin et al., 2007; Kelley et al., 2010). Solid curves are melting paths based on the hydrous mantle melting parameterization (DMM1) of Kelley et al. (2010) for the labeled arc segments at the average pressures (GPa) and temperatures (ºC; where T_o is the dry solidus) determined using the Lee et al. (2009) geothermobarometer.

Additional References (not in text):

Salters, V.J.M., Stracke, A., 2004. Composition of the depleted mantle. Geochem, Geophys, Geosys, 5(5), Q05004, doi:10.1029/2003GC000597.

Workman, R.K., Hart, S.R., 2005. Major and trace element composition of the depleted MORB mantle (DMM). Earth Planet. Sci. Lett. 231: 53-72.